

https://dspace.org/

Radioactivity assessment of Uranium Isotopes concentration in water sources near selected former uranium mines in the West-Rand area of Johannesburg

Mohlala, Nthabiseng

2022

https://hdl.handle.net/10539/34573

Downloaded from a DSpace repository. https://dspace.org/

Radioactivity assessment of Uranium Isotopes concentration in water sources near selected former uranium mines in the West-Rand area of Johannesburg

Nthabiseng Mohlala

A dissertation submitted to the Faculty of Science, University of the Witwatersrand, Johannesburg,
in fulfilment of the requirements for the degree of
Master of Science.

May 4, 2022

Supervisor: Prof. Iyabo Usman (University of the Witwatersrand)
Co-supervisor: Prof. Ivo Petr (University of the Witwatersrand)

Declaration

I hereby declare that this that this thesis represents my individual research, and all contributions from external sources have been accurately identified with appropriate citations to the literature, and acknowledgement of the research and discussions. It is being submitted for the Degree of Master of Science at the University of the Witwatersrand, Johannesburg. It has not been submitted before for any degree or examination at any other University.



07/12/21

Abstract

This dissertation investigated the activity concentration levels of uranium isotopes in water samples collected in the West Rand-area of Johannesburg. One of the primary goals was to determine if the public dose limit of 1.0 mSv/y was not exceeded. Dose rates were calculated according to the National Nuclear Regulator [1] RG-002, consumption rate for different age groups and dose conversion factors published in IAEA General Safety Requirements Part 3 were used. Dose was modeled for various age groups to ascertain the contribution of the uranium isotopes to the total dose of a person consuming the water on a regular basis. Measurements of uranium isotopes were conducted by using Alpha Spectroscopy system from Canberra with Passivated Implanted Planar Silicon (PIPS) detector and Inductively Coupled Plasma Mass Spectrometer (ICP-MS) technique for measurement of isotopic elements.

Based on the results presented for the water samples collected for this study, the quality of water from mining areas varied with fairly high activities measured in some surface water samples from the gold mine areas. The highest activity of 1300±24.7 mBq/l being measured from Blyvooruitzich (Bly4) sampling point collected in June 2019. Downstream of Gold mining operations of Driefontein sampling point recorded marginally lower activity concentration of 142±8 mBq/l was observed in March 2020. The ratio of $^{234}U/^{238}U$ was found to be equal to one, which indicate that the water was impacted by the mining activities. The estimated annual effective dose for all the age groups were well below the National Nuclear Regulator dose constraint of 0.25 mSv/a. The current study found that the annual ingestion dose of ^{234}U, ^{235} and ^{238}U were less than the World Health Organization recommended levels of 1 Bq/l and 1 Bq/l and 10 Bq/l,in drinking water [2].

From June 2019 through March 2020, average values of annual effective dose for uranium isotopes were 3.62E-02 mSv/a, 3.51E-02 mSv/a, 3.41E-02 mSv/a and 2.91E-02 mSv/a respectively. Bly4 measured the highest annual effective dose of 9.17E-02 mSv/a in sample collected June 2019 (Winter season)

for 15 years age groups.

Uranium 238 levels exceeded the Target Water Quality Range (TQWR) of 0.89 Bq/l as provided by the Department of Water and Sanitation for all the sample collected at Blyvooruitzich (Bly4), Blyvooruitzich combination and Peter Wright outlet. This means the annual cancer risk is less than one in a million. All the other sampling points were lower than the TQWR, this implies that there is no significant effects. There is no statistical significance in comparing the mean values of two groups.

Dedication

To my parents, my late Aunt Sthandos, who has always backed me up and encouraged me to try new things,

Acknowledgements

Throughout the writing of this dissertation, I received a lot of help and encouragement. Sincere thanks go to the Almighty God for making this thesis a success. I wish to thank most deeply my supervisor, Dr Iyabo Usman and Prof. Ivo Petr, who have provided without hesitation, constructive feedback, recommendations, and critiques, all of which have provided support to this Masters Research project. I wish to express my deepest gratitude to Dr Uwais Ahmed and Dr Shikweni who inspired me to pursue the Master Degree.

I would like to express my sincere gratitude to National Nuclear Regulator (NNR) and Centre of Nuclear Safety and Security (CNSS), for providing financial assistance and giving me the opportunity to pursue my studies.

I would also like to thank Dr. Mkhosi and Mr John Pule, for their valuable guidance throughout my studies. You provided me with the tools that I needed to choose the right direction and successfully complete my dissertation. Kudus to the personnel from the Environmental Surveillance Laboratory at NNR, L. Mkhize, O. Moya, Q. Mahlangu and M. Segaole for their valuable assistance and dedicated work in performing the measurements. Similarly, I am grateful to RITS Management, especialy Mr A Muller.

In addition, I would like to express my gratitude to my parents for their sound advice and sympathetic ear. You are always willing to help me. Finally, I could not have finished this dissertation without the help of my family, particularly my husband Mr. James Rambao, who provided stimulating discussions as well as enjoyable distractions from my study. My children, Naledi and Mukhethwa Rambao, for their love and support, as well as their patience as a working mother.

Contents

Declaration ii

Declaration ii

Acknowledgements vi

List of Figures xi

List of Tables xiii

1 Introduction 1

1.1 Background 1
1.2 Problem statement 2
1.3 Aim and Objectives 4
1.4 Dissertation arrangement 5

2 Literature Review 6

2.1 Uranium Mining in South Africa 6
2.2 Studies of uranium around mining areas 9
2.3 Exposure pathways 10
2.4 Radioactivity 12
2.4.1 Radioactivity decay 13
2.4.2 Radioactive decay chain 17
2.5 Secular Equilibrium 19
2.6 Interaction of radiation with matter 20
2.6.1 Photoelectric Effect 21
2.6.2 Compton Scattering 22
2.6.3 Pair Production 23
2.7 Alpha particles interaction with matter 23
2.8 Biological effects of ionizing radiation 27
2.9 Radiation Exposure and Dose 29

2.9.1 Absorbed dose 29
2.9.2 Effective dose 30
2.10 Excess lifetime cancer risk 31

3 Experimental Methods **32**
3.1 Study Area 32
3.2 Materials and Methods 34
3.2.1 Sample collection and treatment 34
3.2.2 Sample preparation 38
3.2.3 Alpha source preparation methods 39
3.2.4 Alpha source preparation used for present study 42
3.3 Measurements Techniques 44
3.3.1 Alpha Spectrometry system 47
3.3.2 Calibration of Alpha Spectrometer 50
3.3.3 ICP-MS measurements 54
3.4 Detection systems 55
3.4.1 Solid-sate Detector 56
3.4.2 Silicon and Germanium detectors 57

4 Results, Analysis and Discussions **60**
4.1 Overview of uranium isotopes activity 60
4.2 Pb, Bi and Th elemental composition in the measured samples . 69
4.3 Uranium Isotopes Dose Assessment 70
4.3.1 Annual dose criteria 71
4.3.2 Dose Evaluation 72
4.3.3 Excess lifetime cancer risk 74
4.4 Statistical analysis of results 81

5 Conclusion **83**
5.1 Recommendations 84

Bibliography **94**

A Anova Analysis **95**

List of Figures

2.1 Natural decay chain of Uranium series showing different daughter nuclides taken from Ref [14] 8
2.2 Potential exposure pathways, main environmental pathways of human radiation exposure (taken from Ref.[24]) 11
2.3 A schematic diagram of an alpha decay 14
2.4 Photoelectric effect within an atom (taken from [42]) 21
2.5 Schematic diagram of Compton scattering showing the relationship of the incident photon and electron initially at rest to the scattered photon and electron with a given kinetic energy (taken from Ref. [43]) 22
2.6 The schematic diagram of the pair production (taken from Ref. [43]) 23
2.7 The range of alpha particle in silicon, used from reference (taken from [29]) 25
2.8 Shows radiation source damaging the DNA of the cell, leading to cell division in an uncontrolled manner to cause cancer (taken from [43]) 27
2.9 Direct and indirect damage examples (taken from [37]) 28

3.1 Geological map showing West Rand Goldfield where the current investigation was conducted (taken from Ref.[53]) 33
3.2 the population pyramid for the West Rand District (taken from Ref. [54]) 33
3.3 A picture taken during water sampling activities 36
3.4 Picture taken of the contamination monitor used with its calibration certificate 37
3.5 Prepared water sample designate storage area 37

3.6 LHS: Typical micro-precipitate deposited by filtration with radionuclide (s)on a fine porous size membrane filter paper RHS: Prepared filtration funnel with 0.1 µm polypropylene and 25 mm in diameter . . . 39
3.7 LHS: Source prepared on a stainless steel disc RHS: Schematic diagram of the electrodeposition cell (taken from Ref.[60]) . . . 41
3.8 Pictorial representation of chemical separation set-up using UTEVA resin . . . 43
3.9 Schematic diagram illustrating stages of methods involved in uranium sample preparation for alpha spectrometer measurements 43
3.10 Alpha Spectroscopy Vacuum pump . . . 49
3.11 Alpha Spectroscopy from Canberra with 12 chambers . . . 49
3.12 Canberra Alpha Analyst spectrometer situated at NNR Environmental Laboratory . . . 50
3.13 The standard radionuclide source prepared by electrodeposition onto a stainless steel disk . . . 51
3.14 Energy calibration curve for the standard source for the PIPS detector . . . 52
3.15 Picture illustrating the Energy efficiency on the Alpha Spectrometer . . . 53
3.16 A schematic diagram of ICP-MS (taken from [71]) . . . 55
3.17 A schematic diagram of an alpha spectrometer (taken from [43]) 59

4.1 June 2019 Activity concentration results for uranium isotopes considered . . . 65
4.2 September 2019 Activity concentration results for uranium isotopes considered . . . 65
4.3 December 2019 Activity concentration results for uranium isotopes considered . . . 66
4.4 March 2020 Activity concentration results for uranium isotopes considered . . . 66
4.5 Percentage contribution to the total uranium isotopes activity concentrations in water samples in the four surveyed seasons in the current study. . . . 67
4.6 Uranium 234 Activity concentration results for all seasons at different sampling areas . . . 67
4.7 Uranium 238 Activity concentration results for all seasons at different sampling areas . . . 68

4.8 Estimated total doses from uranium isotopes for different age groups for June 2019 77
4.9 Estimated total doses from uranium isotopes for different age groups for September 2019 results 77
4.10 Estimated Total dose for uranium isotopes for different age groups for December 2019 results 80
4.11 Estimated Total dose for uranium isotopes for different age groups for March 2020 results 80
4.12 Bar graph showing ELCR fo uranium isotopes in water samples at different mining locations in West-Rand area 81

List of Tables

3.1 Origin and sample information of the samples under investigation 35
3.2 Calibration source with corresponding activity concentrations and photo-peak energies 52
3.3 Counting efficiency using the calibration source 53

4.1 ^{234}U, ^{235}U, and ^{238}U activity concentrations in water samples from the study area. 64
4.2 Isotopic concentrations of ^{208}Pb, ^{209}Bi and ^{232}Th in the measured samples. 70
4.3 Dose conversion factors (Sv/Bq) used to calculate human ingestion dose and Annual Consumption – humans L/a. 72
4.4 Calculated standard deviation for the annual doses for the study area. 74
4.5 Excess Lifetime Cancer Risk (ELCR) for ingestion of uranium isotopes for 15 years age group. 75
4.6 Radiation dose classification for drinking water with health effects and intervention time frames indicators. [88] 76
4.7 Annual dose (mSv/a) calculated for June 2019 and September 2019 water samples. 78
4.8 Annual dose (mSv/a) calculated for December 2019 and March 2019 water samples. 79

A.1 Uranium 234 activity concentration (mBq/l) from June 2019 to March 2020 in water samples. 95
A.2 Uranium 238 activity concentration (mBq/l) from June 2019 to March 2020 in water samples. 96
A.3 Uranium 235 activity concentration (mBq/l) from June 2019 to March 2020 in water samples. 96
A.4 Calculated annual effective dose in mSv/a June 2019. 97
A.5 Calculated annual effective dose in mSv/a Sep 2019. 97

A.6 Calculated annual effective dose in mSv/a December 2019. . . . 97
A.7 Calculated annual effective dose in mSv/a March 2020. 98

Chapter 1

Introduction

1.1 Background

The focus of this project is based primarily on the uranium isotopes activity concentration in the water sources from Uranium mines. Water used for consumption may contain radionuclides at activity concentrations that cause health problems for humans. This study evaluated the concentrations of uranium in the different streams of water associated with water for human consumption, water used for irrigation of farmlands and the mineral processing water discharged near mining sites.

SANS 241 (South African National Standard) was used in this study to assess the quality of drinking water [3]. By analysing the activity concentrations of uranium in the different water samples collected within the study area of West Rand, guidance could be provided for reducing health risks.

Uranium activity concentrations differ over a wide range due to natural activities and physical location of water areas (in different types of soil, rocks and biological characteristics) and also varies over climatic characteristics. Naturally occurring radionuclides occur in three decay series, with the main being Uranium-238, Thorium 232 and Uranium- 235, as shown in Figure 2.1. Uranium and thorium are radionuclides with long half-lives, their abundances in the earth's crust are 2.5 ppm for both the radionuclides. In nature, the radionuclides in these three series are approximately in a state of secular equilibrium between the parent nuclide and daughter nuclide, in which the activities of all radionuclides within each series are nearly equal.

The isotopes ^{238}U and ^{234}U are in a state of secular equilibrium, as they are separated by two shorter-lived radionuclides, ^{234}Th and ^{234}Pa. The decay process itself, allows some dissociation of the decay radionuclide from the source material, facilitating subsequent environmental transfer. Thus, ^{234}U may be somewhat deficient relative to ^{238}U in soils and enhanced in rivers and the sea. The radionuclide ^{226}Ra in this chain may have slightly different concentrations than ^{238}U, because separation may occur between its parent radionuclide ^{230}Th and uranium and because radium has greater mobility in the environment. The decay products of ^{226}Ra include the gaseous element radon, which diffuses out of the soil, reducing the exposure rate from the ^{238}U series [4].

In a previous detailed study reported in the Mooi River Study, only two pathways for causing extreme potential exposures were revealed: intake resulting from regular and continuous use of the water for drinking purposes, and regular consumption of fish obtained from the proposed contaminated water bodies. In terms of the latter, there is relatively little data on radionuclide bioaccumulation rates in local fish species, and international experience reveals that bioaccumulation rates can vary by three orders of magnitude. As a result, more research into the fish pathways is required. Tailings in the study area are a major source of uranium pollution in the environment [5]. They represent a major potential source of uranium pollution in water. There has been an increase in uranium content at all mines that have abandoned uranium production since the 1980s. According to projections of the entire surface area covered by tailings dams, rainfall volumes, and the rate at which uranium is leached from tailings particles, unlined tailings dumps alone release around 50 tons of dissolved uranium yearly into the environment. Seepage from such tailings, which flows through the groundwater is a main source of water contamination in the area and is difficult (and expensive) to prevent. The mines in Gauteng and the North West contain toxic radioactive nuclides such as radium, polonium, thorium, and uranium, as well as certain lead isotopes.

1.2 Problem statement

Water is an essential component of natural resources and plays a major role as it is a need of life, for drinking, irrigation, and aquaculture and livestock

usages. Internal exposure to radioactive pollutants from water occurs mostly by ingestion, either directly or indirectly through eating biota that have taken up the water.

The impact of gold mining regarding water resources, affect the availability of water and the quality of the water. There is also a great concern in many parts of the world regarding water crisis. South Africa is facing water crisis, not only because of the scarcity of water, but also the quality of the available water due to the mining activities. The mine tailings and waste rocks contribute to the contamination of the water resources and are of particular concern. In the West Rand and Far West Rand goldfields, about 100 000 tons of uranium are estimated to be present in the tailings deposits. Exposing the treated ore from underground to the much more chemically aggressive environment of an atmosphere with free oxygen and water often leads to an increased release of leached heavy metals from the tailings particles, for example by acid mine drainage.

Approximately 1.6 million people live in close proximity of the tailings dam in Gauteng Province, and also growing informal settlements are moving closer and closer to the tailings dam, this was reported in the Gauteng Department of Agriculture and Rural Development, 2009 final report [6]. Due to lack of piped water, members of the public in areas adjacent to the mines and downstream of the mines use stream water for drinking purpose. The stream water is also used to water the livestock and to irrigate the crops. Most residents in the West Rand area may have access to water either from the streams or boreholes contaminated by these radionuclides. Other sources of possible release of contaminated water may include run-off from contaminated surfaces such as slimes dams, rock dumpsites, high-grade ore piles, metallurgical plants, etc., leakages from cracked canals or pipelines, seepage from unlined return-water dams and evaporation facilities containing highly contaminated process water, etc., as well as spillages from recovery plants.

The assessment of the impact radioactivity in the environment have been conducted in the past. These studies were carried out to assess the levels of radioactivity in water sources from uranium mining and processing. The study conducted by the Institute for water quality in 1999, concluded that Mining activities are a major contributor to uranium and uranium series radionuclides

within the catchment area in the West Rand area [7].
The study by Henk Coetzee et al [8] showed that the uranium accumulates in the river sediments and soil in the West rand area. This has a serious negative impact on the vegetation surrounding the water bodies, and may pose a serious threats to the farming industry next to the mining areas. ^{238}U and its progeny radionuclides ^{234}Th, ^{234}Pa, ^{234}U, ^{230}Th, ^{226}Ra, ^{222}Rn, ^{218}Po, ^{214}Pb, ^{214}Bi, ^{214}Po, ^{210}Pb, ^{210}Bi and ^{210}Po are alpha and beta emitters. These radionuclides can cause damage to the tissues [8]. These elements may also be absorbed in the skin, in particular, absorption of uranium through ingestion may lead to destruction of the kidney, which can affect the neurological system causing blindness, paralysis and loss of coordination.

According to the study in [8], the sediments in the Andries Dam in the Blyvooruitzicht which receive water from Wonderfonteinspruit, contains uranium of about 900 mg/kg. Approximately 1100 mg/kg were detected in the sediments samples collected in the upper Wonderfonteinspruit. As a result, the use of water for drinking or irrigation purposes may pose a serious health risks to the members of the public residing near the water bodies. In light of earlier studies on environmental radioactivity, this research was undertaken with the primary goal of determining the radiation levels of uranium isotopes in water samples collected near mines in the West Rand.

1.3 Aim and Objectives

The aim of this study was to assess the radioactivity levels of uranium isotopes in waters sources in the West Rand mining area. The specific Objectives were to:

- Evaluate the radioactivity level of Uranium isotopes in drinking water from the study area.
- Estimate the Dose levels in the water due to exposure to NORM from drinking water
- Model Effective doses for different age groups with respect possible release of Uranium isotopes in the environment for both drinking and mining related processed water.

1.4 Dissertation arrangement

The following is the arrangement of this dissertation:

Chapter 1 introduces the context and the objectives related to this study

Chapter 2 describes the necessary theory and descriptions associated with Uranium isotopes. This chapter also covers health effects related to radiation protection and the dose limits.

Chapter 3 provide a brief discussion of the relevant measuring techniques and methods used for Uranium activity concentration determination.

Chapter 4 outlines experimental results obtained as well as discussion on health effects of estimated doses to the public.

Chapter 5 summarises the main conclusion of the dissertation and draws several recommendations that can be considered for future research.

Chapter 2

Literature Review

The work at hand was aimed at the quantification of the activity concentration for uranium isotopes in water samples collected at different location at West-Rand Area of Johannesburg. This chapter discusses the origin of the Uranium isotopes and their propagation in nature. In addition, applicable theoretical aspects in understanding radioactivity as well as major radiation protection concepts is addressed.

2.1 Uranium Mining in South Africa

Uranium can be found mostly as a trace element in the natural environment, however, mining of uranium-bearing ore often transfers high concentrations of the radionuclide from the 'safe' geological underground into the biosphere. In South Africa uranium is brought to the surface mainly by gold mining, since both metals are commonly associated with mined auriferous ore bodies ('reefs') of the Witwatersrand [5]. In the case of natural environment, mining and milling of uranium ore has the potential risk of causing environmental pollution of nearby watercourses, reduced ecosystem viability and biodiversity and aquifers by radionuclides, heavy metals and other contaminant [9].

Uranium mining and milling tailings are of particular environmental concern because of the following fundamental reasons [9]:

- Their radioactivity is very long lived,
- They retain much of the radioactivity of the ore from which they were derived,

- The common method of surface disposal exposes a large surface area to the natural elements and thus increases the risk of release of radiation flux, radioactive and geochemically toxic dusts, and interaction with surface water systems,

- The large surface area of these generally thin tailings deposits (or 'piles') adversely affects large areas of land and renders potentially valuable land unfit for other uses.

Johannesburg sits on the edge of the world's largest known gold deposit. Mining was opened to the public in 1886, where the world's largest deposits were found on the Witwatersrand basin. After a few years, the city was the largest settlement in South Africa and migrant workers swelled from across Southern Africa and beyond. Mining operations spread along extensions of these deposits in the Central Rand, West Rand and East Rand Gold fields and beyond.

While gold mining is still continuing in these areas until today, the gold mining industry in South Africa is in a mature state. Considerations about mine closure and the legacies of mining operations take a prominent position among government sectors as well as corporate companies. West Rand gold reefs southwest of Johannesburg, is partitioned into several groundwater compartments by predominantly north–south trending syenite dykes. The primary water flow was westwards before mining, decanting over dyke boundaries as a succession of springs along the lower Wonderfontein Spruit [10].

Extraction of water from mines and decant from abandoned mines have a major negative impact on the quality of the surface water and groundwater in Gauteng [11]. Uranium is a naturally occurring element in the Earth's crust, with an average concentration of 2.5 ppm, and it can be found practically everywhere. Uranium activity concentrations differ over a wide range due to natural activities and physical location of water areas (in different types of soil, rocks and biological characteristics) and also varies over climatic characteristics. Radioactive substances depending on their origin are divided up into two groups; natural and anthropogenic.

Natural Uranium is composed of three major radioisotopes which decay by both alpha and gamma emissions, i.e. ^{238}U, ^{235}U and ^{234}U, with ^{238}U being the most prevalent isotope. ^{238}U has a half-life of approximately 4.47 billion

years; ^{235}U a half-life of 704 million years and that of ^{234}U being 245 500 years; making them suitable for dating the age of the planet. Natural Uranium contains 99.284% ^{238}U, 0.711% ^{235}U, and minute of ^{234}U by weight 0.0055% [12]. Approximately 2.2% of its radioactivity comes from ^{235}U, 48.6% from ^{238}U , and 49.2% from ^{234}U [13]. Other naturally occurring radionuclides, including ^{40}K (potassium), and those originating from the thorium and uranium decay series, in particular, ^{226}Ra, ^{228}Ra, ^{234}U, ^{238}U, ^{210}Pb, can be found in water for natural reasons, this includes

- desorption from the soil and wash-off by rain water,
- released from rocks and minerals which forms the aquifer as happens with other cations and anions,
- released from technological processes involving naturally occurring radioactive materials (e.g. mining and processing of mineral sands or phosphates fertilizer production and use),
- weathering of igneous rocks that formed the Earth's original crust.

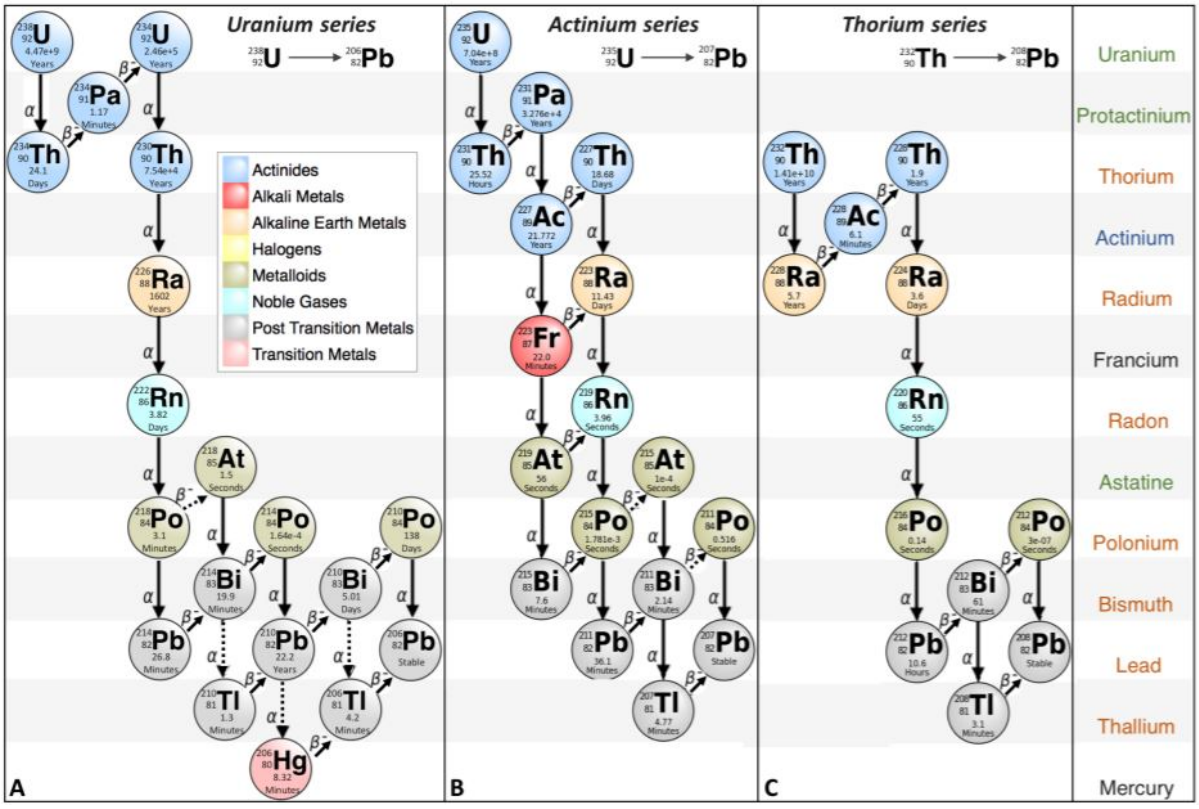

Figure 2.1: Natural decay chain of Uranium series showing different daughter nuclides taken from Ref [14]

2.2 Studies of uranium around mining areas

In 2001, a study on uranium and radium in groundwater and surface water samples was undertaken in Morocco [15]. The activity concentrations and activity ratios of uranium isotopes and radium isotopes were determined in this study for 15 wells, 14 hot springs, 7 cold springs, and 11 rivers. Radium isotope activities were measured using ultra gamma spectrometry with a low background and high efficiency well type germanium detector, while uranium activities were counted in an alpha spectrometer. The average activity concentrations were discovered to range between 7.86 to 163.06 mBq/l for ^{234}U, and for ^{238}U the activity concentration ranged from 9.99 to 27.86 mBq/l. It was concluded that the results show that none of the sources cause significant radiation pollution. The activity concentrations determined in Ref. [15] are lower as compared to the results presented in this dissertation.

Department of Water and Sanitation undertook another study in the Klip River catchment as reported in [16]. The majority of the tested water samples in this study had a blue water quality (0.1 mSv/a), however water from eight sites had a green water quality (0.1 to 1.0 mSv/a). For the most sensitive newborn age group, two of these sites had a dosage of >0.25 mSv/a. At three locations, possible significant uranium chemical toxicity concentrations were measured. According to this investigation, the dose near the Klip River's lower end was similar to the natural background radiation. Also because Klip River flows into the Vaal river, which is widely used for drinking water, this was critical for the work.

Another investigation was carried out during 2014 in Tano North district, Ghana [17].The activity concentrations of radionuclides in water, soil and tuber crops were investigated. A total of forty water samples were collected from boreholes, wells, and streams. The measurements were made using a gross alpha/beta spectrometry system with a low background gas-free automatic alpha/beta counting system. The concentrations of gross alpha/beta activity in water ranged between 0.007 and 0.039 Bq/l, while uranium 238 concentrations ranged between 0.23±0.02 and 0.38±0.02 mBq/l. The average annual effective dose due to NORM ingestion in water by the human popula-

tion was approximately 50 micro Sv/a.

The radiation levels of naturally occurring radioactive materials in the operational region of the Akyem Gold Mine and nearby settlements were measured in 2016 [18]. To quantify the radionuclides of interest, namely ^{234}U, ^{232}Th, and ^{40}K, the radioactivity was measured using direct gamma ray spectrometry for soil samples and gross alpha/beta for water samples. Boreholes, surface water bodies (streams), and mine pits were all used to gather samples. In subsurface tailing water, gross alpha activity concentrations in water samples ranged from 1.25 mBq/l to 4.95 mBq/l. Surface water activity concentrations ranged from 1.20 mBq/l to 42.54 mBq/l in subsurface tailing. All of the gross alpha and gross beta values were found to be lower than the usual values, according to the study (WHO recommendation values).

2.3 Exposure pathways

Being a primordial radionuclide, uranium widely spread in the environment and thus poses a potential radiation risk to human life. It is identified as a major contaminant of concern produced in the gold mining industry. Terrestrial exposure, inhalation and ingestion are the important pathways through which uranium delivers radiation to members of the public [19]. Its impacts, after mine closure, on persons, property, and the environment are, therefore, long term and of appreciable magnitude [20].

The primary pollutant of concern released by the gold mining sector has been identified as uranium [21]. Uranium has a very long half-life and is both radioactive and chemically hazardous. Natural sources is the major source of the ionizing radiation to which the public is exposed to in the environment [22]. The sources include:

- radon gas and its decay products in the atmosphere - natural uranium in soil and rocks, gamma rays from the ground,
- cosmic rays from outer space and,
- naturally occurring radioactivity in foodstuffs and drinking water, also derived from radionuclides in the soil, as well as inhalation of respirable airborne dust

An individual's overall radiation dosage from these natural sources is estimated to be around 2.4 millisieverts per annum (mSv/a). In high background locations, geological and geographical variables can make doses from any of these sources dominate by a factor of ten, according to Ref [22].

The most important pathways to radiation exposure to the public are usually external exposure to gamma radiation, inhalation and ingestions [23].

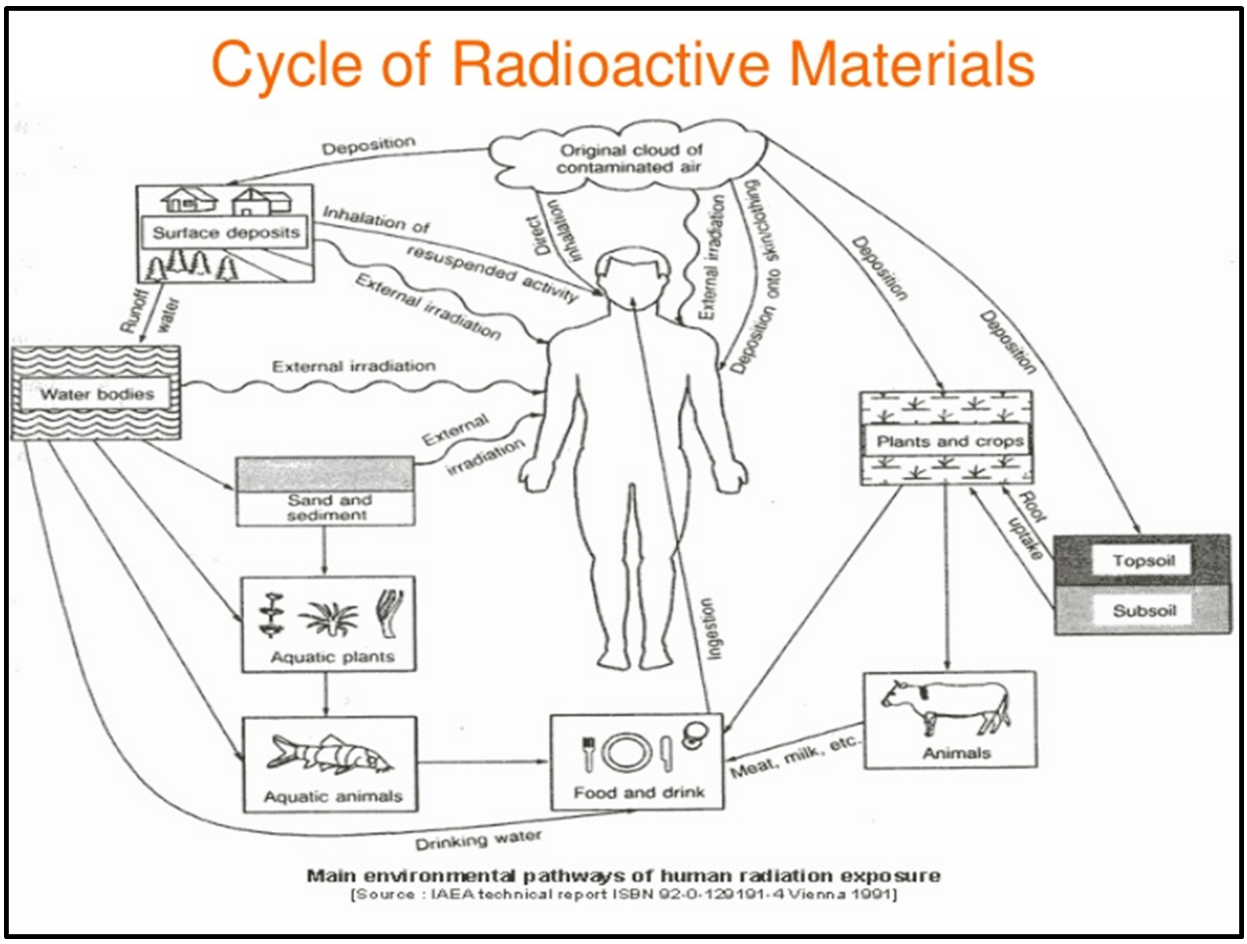

Figure 2.2: Potential exposure pathways, main environmental pathways of human radiation exposure (taken from Ref.[24])

Figure 2.2 illustrates the most important pathways by which human being is exposed to radiation and should be considered for dose calculations. Exposures from water containing radioactive contaminants essentially occur internally through ingestion, either by direct consumption or indirectly by consumption of animal or vegetable products that have themselves taken up the water. Radioactive decay is exponential in time and is based on the transition of

a parent to daughter nucleus and is a statistical process. The disintegration (decay) probability is a fundamental property of an atomic nucleus and remains equal in time. Mathematically this law is expressed as:

$$dN = \lambda N.dt, \tag{2.1}$$

and

$$\lambda = -\frac{dN/dt}{N} \tag{2.2}$$

where N is the number of radioactive atoms, $-dN/dt$ the decrease of this number per unit of time interval and λ (decay constant) is thus the probability of decay per nucleus per unit of time interval. This decay constant is specific for each decay mode of each nuclide.

2.4 Radioactivity

Henri Becquerel discovered the radioactivity of uranium in 1896 [25]. In 1897 he found that thorium was radioactive too, and two new radioactive elements, polonium and radium, were discovered by Pierre and Marie Curie, while a third one, actinium, was identified by André Debierne [26]. At present, out of 118 elements listed in the periodic table, only 94 occur naturally. Elements are identified by according to the number of protons (atomic number, Z) in their atomic nucleus. The number of electrons is equal to the number of protons in an element. However, the same element's atoms may not be the same in the number of neutrons, and atoms of the same atomic number but with different neutron number are called nuclides or isotopes of the same element. The mass of an atom (A) is the sum of all nucleons in the atomic core and N is the number of neutron in the nucleus: A = Z + N [27].

More than 3000 radioisotopes are known, whilst 254 are stable isotopes and about 84 are found in nature. These isotopes can be characterized in an extended form of the Periodic Table known as a nuclide chart [28]. In ref. [29], radioactivity is defined as the spontaneous emission of radiation from a nuclear reaction or as a result of the decay of electromagnetic radiation from unstable atomic nuclei.

2.4.1 Radioactivity decay

The most common kinds of ionizing radiation emitted are produced by the decay of unstable nuclides:

- Alpha (α) decay (Helium nucleus is emitted)
- Beta (β) decay (Electrons are emitted) and,
- Gamma ray decay (High energy photons are emitted).

2.4.1.1 Alpha decay

Alpha particles strongly interact with other atoms in their path, this as a result of their charge and relatively high mass, compared with other kinds of radiation. When compared to other kinds of nuclear radiation, alpha particles are slow and hefty. Alpha particles, because they are highly ionising, are unable to penetrate very far through matter and can only travel a few centimetres in air. And thus, this makes it favourably easy to shield off alpha radiation. However, the strong absorption of α-particles in matter makes them hard to detect and implies special constraints on sample preparation and detector properties. Samples should be homogeneous and sufficiently thin in order to avoid strong alpha absorption in the sample itself (attenuation) [30]. On the other hand, alpha particles can cause multiple ionisations within a very small distance. This gives them the potential to do much more biological damage (inhaled or ingested) for the same amount of deposited energy. Figure 2.3, below shows the process of alpha emission.

Alpha α particles are composite particles and consists of two protons and two neutrons tightly bound together. They are identified as the nucleus of the Helium isotope $^{4}_{2}$He, emitted from the nucleus of some radionuclides during a form of radioactive decay, called alpha-decay. The decay process is as follows:

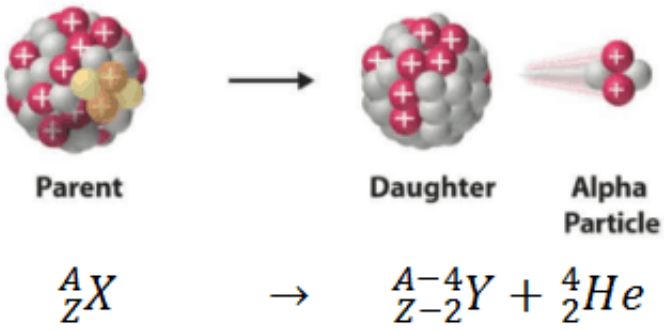

Figure 2.3: A schematic diagram of an alpha decay

$$^{A}_{Z}X \longrightarrow ^{A-4}_{Z-2}Y + ^{4}_{2}He + Q \tag{2.3}$$

An example of decay in nature is the decay of ^{238}U to ^{234}Th. Eq. 2.3 describes this process, where X is the parent and Y is the daughter nuclei, A is the atomic mass and Z is the atomic number [31].

An alpha particle, with its two protons and two neutrons, is a very stable particles. During the alpha decay, an unstable nucleus ejects an alpha particle and decays into a different atomic nucleus. The atomic number is reduced by two while the mass number reduced by four. Alpha particles as well as other types of charged particles breakdown their energy during collisions mainly by two mechanisms: ionization and electron excitation. The high mass and charge of an alpha particle, relative to other forms of nuclear radiation, gives it greater ionization power but a poorer ability to penetrate matter. For elements with high atomic numbers such as uranium, radium, and thorium alpha decay will usually occur. This makes the alpha particle emission possible as the nuclei of these elements are rich in neutrons.

The Q-value of alpha decay, is the difference in the mass of the parent and the combined mass of the daughter and the α-particle. The Q value can be calculated by accounting for the total mass/energy change in the decay process using Eq. (2.4). The mass difference between the parent and daughter nucleus can usually be estimated quite well from the Liquid Drop Model [32]. The model treats the nucleus as a drop of incompressible nuclear fluid of very high density. The Q value must be positive for the decay to take place, otherwise it is not possible for the particle to tunnel through the barrier and escape. The

kinetic energy released in the decay process is distributed between the decay product and the alpha particle, in accordance to the law of conservation of momentum, [33]

$$Q = \frac{1}{2}MV^2 + \frac{1}{2}mv^2, \tag{2.4}$$

Where m and v represents the mass and initial velocity of the alpha particle, M and V represents the mass and the velocity of the recoil nucleus, and therefore. Substituting the velocity $V{=}mv/M$ to Eq. (2.4) leads to

$$V = \frac{1}{2}M\frac{m^2v^2}{M^2} + \frac{1}{2}mv^2 \tag{2.5}$$

Eq. (2.7) represents the alpha particle kinetic energy.

$$E = \frac{1}{2}mv^2 \tag{2.6}$$

The value for Q can be presented as follows

$$Q = E\frac{m}{M} + 1 \tag{2.7}$$

And therefore substitution for Kinetic energy (E) can be presented as per Eq. (2.9) [34].

$$E = \frac{Q}{1 + \frac{m}{M}} \tag{2.8}$$

This equation indicates two particle emission from an initial unstable nucleus at rest, the alpha particle emerges with precisely defined energy. E and Q have precise values. Since the kinetic energy is lower than the Q value, it is most likely that all the energy released in the decay is carried away by the light particle as kinetic energy.

2.4.1.2 Beta decay

During beta decay, electrons or a positron are emitted from a nucleus. Beta decay may be defined as any nuclear decay process whereby the mass number A of the nucleus remains the same and the atomic number Z changes [29]. There are three types of beta decay, the main two types of beta decay are β^- decay and β^+- decay [35]. These two types occur in atoms which are unstable due to an imbalance in the neutron/proton ratio in their atomic nucleus. In the case of a neutron excess in the nucleus, an atom may undergo β^- decay. In this process, a neutron is transformed into a proton by emission of an electron

β^- particle and an antineutrino as depicted in Eq. (2.10).

$$ {}^{A}_{Z}P \longrightarrow {}^{A}_{Z+1}\, D + \beta^- + v^- + \Delta E_{max} \tag{2.9} $$

The maximum energy for beta particle is E_{max}, contrary to alpha particles, beta particles do not have a discrete emission energy. This is because a variable part of the decay energy is carried off by the antineutrino. E_max has an order of magnitude between 0.01 and 100 MeV [29]. Since both the β^-− and β^+− particles do not have discrete emission energies, it becomes more complicated to exactly determine which isotope ejected them during its decay. However, the energy spectrum of β-particles is still characteristic for their emitter, making its identification possible [35].

2.4.1.3 Gamma decay

After radioactive decay, the decay products are often in an excited energy state. The product nuclide in such an excited state either falls directly to the ground state or descends in steps to lower energy states through the dissipation of energy as gamma radiation. Nuclides of the same nuclear configuration but different energy state are called isomers of the same nuclide, and the transition (or decay) from a higher to a lower energy state is referred to as isomeric transition. Gamma rays are emitted in discrete energies corresponding to the energy state transitions a nucleus may undergo when in an excited state. The energy of a gamma ray may be described as the difference in energy states of the nuclear isomers, [29]:

$$ E_\gamma = hv = E_1 - E_2 \tag{2.10} $$

where $E\gamma$ is the gamma ray energy, hv is the energy of the electromagnetic radiation, and E_1 and E_2 represent the energy levels of the nuclear isomers (E_1 mother isomer and E_2 the daughter isomer). The gamma rays energies are mostly in the range 0.1 to 2 MeV. Since γ-ray carries high amount of energy that has no mass or charge, they have enormous penetrating power and require several centimetres of dense material (such lead) to shield them.

They can eject electrons from the hull of atoms they interact with, giving them ionizing properties and thus the ability to damage molecules of living tissue.

2.4.2 Radioactive decay chain

There are three radioactive decay series that exist in nature. They belong to the uranium chain, the actinide group, and the thorium group. This will lead to the stable lead isotopes of ^{206}Pb, ^{207}Pb, and ^{208}Pb, respectively. The neptunium series is a fourth series, which is no longer significant on the earth because of the short half-lives of the species involved [36].

The half-lives of the three primordial isotopes of the natural decay series are much longer than those of their progeny isotopes. Under this condition, the activity of all progeny isotopes will increase to the activity of the original mother isotope to form a steady equilibrium state [37]. The fundamental law of radioactive decay is based on the fact that the decay, i.e., the transition of a parent nuclei to a daughter nuclei, is a statistical process. The radioactivity is defined as the number of disintegration per unit of time

$$A = -\frac{dN}{dt} = -N\lambda, \tag{2.11}$$

Where N is the number of radioactive nuclei, dN/dt decrease (negative) of this number per unit of time, and λ is thus the probability of decay per nucleus per unit of time. This decay constant λ is specific for each decay mode of each nuclide. The radioactivity or decay rate is defined as the number of disintegrations per unit of time: [37]

Equation 2.12 thus leads to

$$N_T = N^0 e^- \lambda t \tag{2.12}$$

Where N_0 and -λN_0 are number of atoms and activity of a given radionuclides with decay constant in a given sample at time t=0, and N_t and -λN_t at time t. The decay constant is, replaced by half-life ($T_{1/2}$) of a given radionuclides, i.e. the time in which the amount of radionuclides activity is reduced by a factor of two,

$$T_{1/2} = \frac{Ln2}{\lambda} \tag{2.13}$$

The parent in some cases decays to two different products by a process called branched decay. These two decay modes can be called a and b, defining the probability of each decay mode as

$$\lambda_a = -\left(\frac{dN_1}{dt}\right)/N_1 \tag{2.14}$$

$$\lambda_b = -\left(\frac{dN_1}{dt}\right)/N_1 \tag{2.15}$$

The total decay rate of N_1 is

$$-\left(\frac{dN_1}{dt}\right)_{total} = -\left(\frac{dN_1}{dt}\right)_a - \left(\frac{dN_1}{dt}\right)_b = N_1\Big(\lambda_{1a} + (\lambda_{1b})\Big) = N_1\lambda_{1total} \tag{2.16}$$

where,

$$\Big(\lambda_{1a} + (\lambda_{1b})\Big) = \lambda_{1,total} \tag{2.17}$$

is the total decay constant. It follows that N_1 decays according to the following law:

$$N_1 = N_1^0 e^{-\lambda_{1total}t} \tag{2.18}$$

Thus, if the activity of the radionuclides is measured in N_1, it would be difficult to distinguish between the two decay modes because total decay constant can only be measured.

The fraction of $\lambda_1 a/\lambda_1 total$ of N_1 decays by mode a, the fraction of $\lambda_1 b/\lambda_1 total$ of N_1 decays by mode b. This shows that the two types of daughter products are $N_2 a$ and $N_2 b$. The formulas describing the accumulation of each of the daughter products are displayed below

$$N_{2a} = N_{2a}^0 + \Big(\lambda_{1a}/\lambda_{total}\Big)N_1^0\Big(1 - e^{-\lambda_{1total}t}\Big) \tag{2.19}$$

$$N_{2b} = N_{2b}^0 + \Big(\lambda_{1b}/\lambda_{total}\Big)N_1^0\Big(1 - e^{-\lambda_{1total}t}\Big) \tag{2.20}$$

Where N_{2a}^0 and N_{2b}^0 are the initial amounts of daughter product N_{2a} and N_{2b} present before the decay of N_1.

$$N_1 = N_1^0 e^{-\lambda_{1total}t} \tag{2.21}$$

If a radioactive nuclide is situated in the Chart of Nuclides far from the stability line (for the light elements at Z=N), the daughter nucleus after radioactive decay is considered to be radioactive. In nature, this occurs with the heavy nuclides in the uranium and thorium decay series. A series of radioactive

decay products follow the original decay of ^{238}U or ^{232}Th. The parent nucleus decays according to the equations of radioactive decay which is outlined below:

$$A_1 = -(\frac{dN_1}{dt}) = \lambda_1 N_1 \tag{2.22}$$

$$N_1 = N_1^0 e^{-\lambda_{1total} t} and A_1 = A_1^0 e^{-\lambda_{1total} t} \tag{2.23}$$

The amount of daughter nuclei is established by two processes, i.e., radioactive decay and radioactive growth by the decay of the parent nuclei, respectively.

$$-\frac{dN_1}{dt} = -\lambda_2 N_2 + \lambda_1 \tag{2.24}$$

The solution of this differential equation is outlined below:

$$N_2 = (\frac{\lambda_1}{\lambda_2 - \lambda_1}) N_1^0 (e^{-\lambda_1 t} - e^{-\lambda_2 t}) + N_1^0 e^{-\lambda_2 t} \tag{2.25}$$

while at both zero activity and zero time N_2^0=0, the results will be as follows:

$$A_2 = \lambda_2 N_2 = (\frac{\lambda_1}{\lambda_2 - \lambda_1}) A_1^0 (e^{-\lambda_1 t} - e^{-\lambda_2 t}) \tag{2.26}$$

The last term represents the decay of the amount of daughter nuclide present at the time t = 0. The ratio between *λ1* and *λ2* is the dominating factor determining the course of the daughter's activity in time.

2.5 Secular Equilibrium

Secular equilibrium is the type of relation between parent and daughter activity that occurs when the half-life of the parent nuclide is infinitely more prominent than that of the daughter nuclide. Secular equilibrium is another way of saying a system has reached steady-state, that is, there is no longer a change in the decay rates of each nuclide. Examples are the relations between the long-living radio-isotopes of uranium and thorium, ^{238}U, ^{234}U and ^{232}Th, and their decay products as shown below.

$$\lambda_1 \ll \lambda_2 \tag{2.27}$$

Equation (2.25) properly describes the parent activity in time, whereas

equation (2.28) turns into:

$$A_2 = A_1^0(e^{-\lambda_1 t} - e^{-\lambda_2 t}) \tag{2.28}$$

or for $\lambda_1 = 0$

$$A_2 = A_1^0(1 - e^{-\lambda_2 t}) \tag{2.29}$$

Describing the growth of the daughter activity in time if we take $A_2 = 0$ at the beginning. At the end at t $\longrightarrow \infty$, $\lambda_2 t \longrightarrow \infty$ as shown in equation (2.30).

And thus, the daughter activity reaches the activity values of

$$A_2 = A_1^0 e^{-\lambda_1 t} = A_1 \tag{2.30}$$

whereby the activity value of the decay product equals that of the parent (parent and daughter activity value become equal).

2.6 Interaction of radiation with matter

According to the properties of charged particles, radiation is detected by its interaction with matter. The interaction of radiation with the detection medium provides a read-out signal, which is recorded by the detection system. Both the type and energy of incoming particles depends on the interaction methods [38]. Radiation detection often involves electrons, photons or atomic and molecular excitation. The critical mechanism on which radiation detectors are based is the dissipation of a fraction of the incoming radiation energy inside the detecting material. Alpha and beta particles interact through the coulomb force with electrons in a medium through which they pass [39]. The electron feels an impulse from the Coulomb force as the particle passes its vicinity. Depending on the vicinity of the encounter, this impulse may be enough either to elevate the electron to a higher shell: excitation (soft collision) or obliterate it from the atom by ionization (hard collision).

The key parameter of the interaction between radiation and matter is the mean energy deposited per unit mass, according to the fundamental quantitative assumption. All types of radiation can cause this energy deposition, and the unit of measurement is joules [40]. Because photons do not have an electrical charge, their interaction with matter differs from that of charged particles. They do not continuously lose their energy when they pass through matter. The possibility of a photon interacting depends upon, the photon energy, the atomic number and density of the material (electron density of the absorbing

matter). According to Ref. [39], interaction of photon with matter can occur in three different ways: Photoelectric effect, Compton scattering (incoherent scattering) and Pair production .

2.6.1 Photoelectric Effect

Photoelectric effect occurs when a photon interacts with a bound electron in an absorbing medium. An atom may completely absorb the photon energy. The photon energy is transferred to an electron of the atom, and the electron is released, resulting in the formation of an ion pair. Photoelectric absorption predominates for low-energy gamma rays up to several hundred keV, (10 to 100 keV) [41]. Energy of the emitted electron is equal to the energy of the impinging photon less the binding energy of the electron [29]. The photo-electron appears with an energy given by

$$E_e = hv - E_b \tag{2.31}$$

where hv is the energy of the incident photon energy, E_b is the binding energy of the photonelectron in its original shell [39]. The emission of the photonelectron originates from the K-shell of the atom. The process is shown in Fig. 2.4 below.

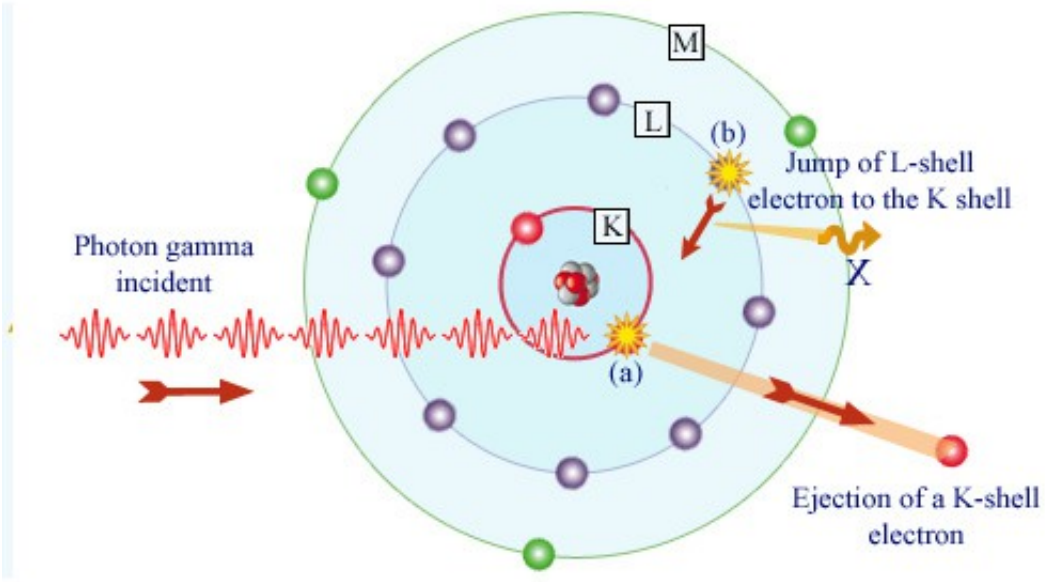

Figure 2.4: Photoelectric effect within an atom (taken from [42])

2.6.2 Compton Scattering

Compton scattering or Compton Effect is a second mechanism by which a photon interact with matter, thus by transferring its energy to an atomic orbital electron. Compton scattering occurs as a result of the interactions of gamma ray or x-ray, with free electrons. In this interaction as shown in Fig.2.5 below, the resultant incident photon is scattered and imparts only a fraction of its energy to the recoil electron. The possibility of the Compton scattering per atom of the absorbing material, depends on the numbers of electrons available as scattering targets and therefore increases linearly with Z [39].

The scattered photon will have a different wavelength and thus a different energy $E{=}hc/\lambda$. Energy and momentum are conserved in this process. The wavelength change of the scattered photon can be determined at an angle θ of the scattered photon. Thus, the energy of the scattered photon decreases with increasing scattered photon angle. The outcome of this interaction is the formation of an ion pair similar to photoelectric effect. However, the scattered photon continues travelling through matter until it dissipates its entire kinetic energy, by interacting with other electrons in a similar fashion [29]. Figure 2.5 illustrate the schematic diagram for Compton scattering taken from Ref. [43].

$$h\upsilon = 2mc^2 + E_{e^-} + E_{e^+} \tag{2.32}$$

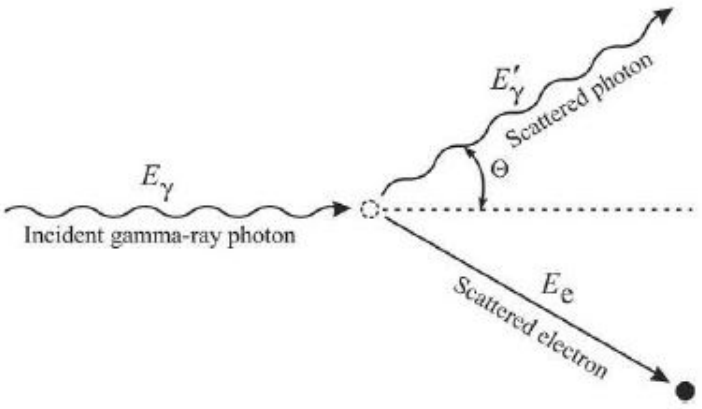

Figure 2.5: Schematic diagram of Compton scattering showing the relationship of the incident photon and electron initially at rest to the scattered photon and electron with a given kinetic energy (taken from Ref. [43])

2.6.3 Pair Production

The third significant way whereby gamma rays interact with matter is by pair production. The photon in this process, interacts with an electron or a nucleus producing a positron-electron pair. TThe minimum gamma ray photon must have an energy of 1.02 MeV for the pair production to be produced. Pair production predominates for high-energy gamma rays of about 5-10 MeV [41]. In pair production, gamma ray energy in excess of 1.02 MeV is imparted and shared equally by the positron and electron as kinetic energy which is given by

$$h_v = 2mc^2 + E_{e^-} + E_{e^+} \tag{2.33}$$

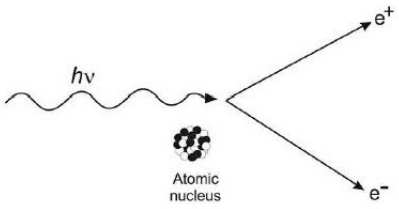

Figure 2.6: The schematic diagram of the pair production (taken from Ref. [43])

2.7 Alpha particles interaction with matter

Different types of radiation interact with matter in different ways. Knowing how a particle interacts with the sensitive part of the detector helps us to get detailed, precise, and quantitative data on the particle's properties. The primary interaction of the charged particle with matter is inelastic collisions with the atomic electrons of the material. These interactions often occur over the path of the particles, which results in energy loss and deflection of the particles from their incident direction. In Ref. [29], only a few types of radiation detectors have been found to be suitable for accurately determining the energy distribution of alpha radiation.

Knowing the interaction of particle with the detector material in detail allows us to deduce extended, precise and quantitative information about the

particle properties. The most common detectors used nowadays are silicon semiconductor detectors. Other semiconductor detectors are also available such as Surface Barrier Detector, Ion-Implanted Silicon Detector and Gridded Ionisation Chamber in Ref. [29]. In the 1980s Si implanted detectors became available as part of research and development for instrumental improvements in spectrum assessment software for alpha spectrometry in Ref. [32]

Another form of detector, which is an ionisation chamber in which the collector is screened electrically by a grid from the volume in which the alpha-particles deposit their energy and create electron/ion pairs, is the Gridded Ionisation Chamber. Despite the fact that scintillation detectors have low energy resolution in general, the advent of "high-resolution" alpha-liquid-scintillation spectrometers in conjunction with selective chemical separation procedures offers some advantages in alpha spectrometry. According to Ref. [29], the interaction between the alpha rays, and the sensitive part of the detector determines the process of detection of alpha emitting particles by various detectors. When alpha particles enter the thin window of the detector, they immediately get in to contact with the atomic electrons of the detector material. Excitation and ionization are the key outcomes of the interaction. In the latter case, electron and positive ion pairs are created. The high-energy alpha particle will form a large number of electron-cation pairs N in its path through the detector.

N can be expressed as:

$$N = \frac{E_\alpha}{\varepsilon} \tag{2.34}$$

E_α represent the energy of the alpha particle and ε represent the energy required to form one electron-cation pair. Since E_α is in the range of a few MeV, and ε is depending on the type of detector in the range of 1 eV to 100 eV, a single alpha particle can produce 10 000 to 1 000 000 charge carriers, whereas it losing its energy before it is stopped as outlined in Ref. [29]. Because the interacting electrons do not significantly deflect the heavy alpha radiation, the alpha particle trajectory in the detector is practically straight. Bohr was the first to obtain a quantitative account of energy loss, which Bethe and Bloch then generalized for relativistic charged particles. The specific energy loss of the alpha particle, also called the stopping power, is given by from the Bethe formula in Ref. [29] as expressed below:

$$-\frac{dE}{dx} = \frac{4\pi e^4 z^2 ZN}{(4\pi\varepsilon_0)^2 Mev^2}\left[ln\left(\frac{2Mev^2}{I} - ln(1-\beta^2\right) - \beta^2\right] \tag{2.35}$$

It was further outlined in Ref [29], that the interaction of alpha particles with the detector is defined by a range or distance beyond which no particles can penetrate. As illustrated in Fig.2.7 , the range is determined by the alpha energy and the detector type.

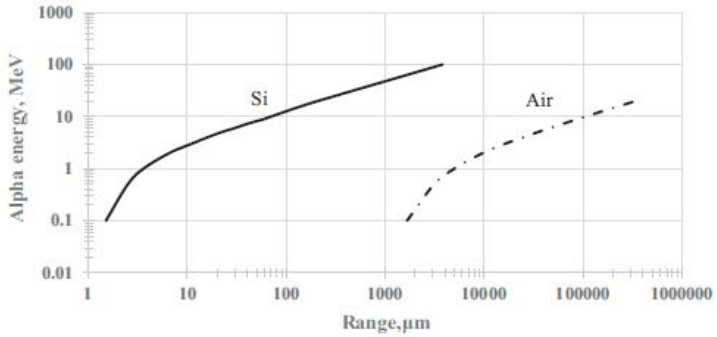

Figure 2.7: The range of alpha particle in silicon, used from reference (taken from [29])

Normally, the emission of alpha particles in detector material or other media is due to electromagnetic interactions of the electrons, but in some cases it can also be caused by atomic interactions, the interactions with nuclei are also likely. The pathway of the alpha rays in these situations do not follow straight trajectory and can back-scatter from the detector, lowering detection efficiency marginally. Because the alpha energy of radionuclides are <10 MeV, a 100 mm thick Silicon layer absorbs them completely. As a result, if silicon detectors are employed to study alpha-emitting radionuclides, they should not be considerably thicker. There are several advantages to using a thinner detector

- More rugged front contact; better energy resolution,
- Lower electronic noise,
- Higher geometric efficiency for some alpha spectroscopy applications, and
- Operation to 60°C and bakeout at 200°C.

Due to the very short range of alpha particles the detector design ensure that the interactions are able to completely absorb the incident radiation, without requiring large detector volumes. However, the limited range of alpha radiation is also responsible for the major challenge in alpha particle detection, which is ensuring that alpha particles reach the active volume of the detector without significant losses. This means reducing or elimination of absorption in the source, any absorbent layers between source and detector, and in the detector window. Absorption and self-absorption in the detection process can be reduced by ensuring direct contact between the source and the detector, for example, by placing the source inside the detector in close proximity of around 1.0 cm. In the case of silicon detectors, in order to reduce the absorption the use of vacuum in the chamber surrounding the detector and the alpha source is recommended [32].

Another step that must be followed is to avoid leaving alpha sources within the vacuum chamber for too long, this is because the sensor can be slowly damaged by the particles themselves. It is also important to be careful to not "contaminate" the measuring chamber with residues of the source, this can be easily done using a disposable aluminum foil as a supporting material,which is a method used at the Laboratory.

Ref. [29] indicated that the interaction of alpha radiation with matter is a statistical process, when mono-energetic alpha particles pass through matter, there is a spread of energies at distances along the beam path, which is called energy straggling. The energy distribution of an originally mono-energetic beam becomes wider with penetration depth; however, towards the end of the range, the distribution becomes narrower again due to the reduction of the beam energy. Analogous to energy straggling, the fluctuation in the path length of the alpha particles due to the statistical nature of the interactions is known as range straggling. Straggling happens in the source, in the media between the source and the detector, as well as in the detector dead layer Ref. [29]. Energy and range straggling are the basic physical processes, which contribute significantly to peak broadening in conventional alpha spectrometry Ref. [29]. Parameters such as characteristics of the detector, the absorbers between the detector and the source, and those of the source affects the peak shape in the alpha spectrometry Ref. [29].

2.8 Biological effects of ionizing radiation

People are being chronically exposed to natural radiation as well as to man-made sources of radiation. High levels of natural background radiation can be found in some regions of the globe such as in Lambwe, South-western Kenya [44], Ramsar in Iran and Gaurapari in Brazil [45]. Residents living in these high background radiation areas receive a high life time dose due to chronic low-level dose of radiation from environmental radioactive elements. Man-made sources of ionizing radiation are widely used as diagnostic tools and therapeutic agents in treatment of diseases. The cumulative exposure to ionizing radiation has the potential to cause harmful health effects leading to chronic diseases [45].

Concerns about the effects of radioisotopes on biological systems have grown as their use has risen. When this radiation comes into contact with living cells, it may produce heating, chemical bond breaks, and molecular ionization. The most severe biological effect occurs when these radioactive emissions fragment or ionize molecules. The energies of both the alpha and beta particles released during nuclear decay events, for example, are substantially higher than the energies of typical chemical bonds. These particles produce extremely reactive ions and molecular fragments whenever they interact with and penetrate materials. Damage to biomolecules in living beings can cause substantial disruptions in normal cell functions, affecting the organism's repair mechanisms and perhaps resulting in disease or death as illustrated in Fig. 2.8 below.

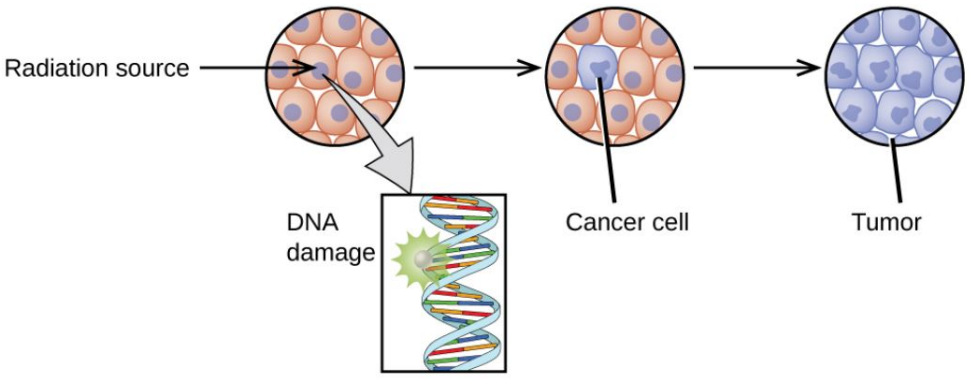

Figure 2.8: Shows radiation source damaging the DNA of the cell, leading to cell division in an uncontrolled manner to cause cancer (taken from [43])

The damage in the viable cell is usually repaired if the cell is not killed but merely modified by the radiation. If the repair isn't perfect, the mutation will be passed down to daughter cells, potentially leading to cancer in the exposed person's tissue or organ. Hereditary illnesses may develop if the cells are preoccupied with transferring genetic information to the exposed individual's progeny. Such consequences in individuals or their offspring are referred to as "stochastic," which means "random"[46].

The biological effects of non-ionizing radiation (for example, light and microwaves) and ionizing radiation, which includes emissions powerful enough to knock electrons out of molecules (for example, particles, rays, X-rays, and high-energy UV radiation), differ significantly. The energy absorbed from non-ionizing radiation causes atoms and molecules to move faster, which is the same as heating the sample. Although biological systems are heat sensitive (as we know from touching a hot stove or spending a day in the sun), a substantial amount of non-ionizing radiation is required before harmful levels are achieved. Ionizing radiation, on the other hand, can cause considerably more serious harm to biological molecules by breaking bonds or removing electrons, altering their structure and function [47]. Indirect harm can be caused by ionizing H_2O (the most abundant molecule in living organisms), which produces an H_2O+ ion that combines with water to make an H_3O+ ion as shown below.

The hydroxyl radical is particularly reactive because it has an unpaired electron. Any material containing unpaired electrons is referred to as a free radical. This hydroxyl radical can react with a wide range of biological molecules such as DNA, proteins, enzymes, etc. This can result in a molecular damage and disruption of physiological processes citevertes2010handbook. In the diagram below, examples of direct and indirect damage are illustrated in Fig. 2.9.

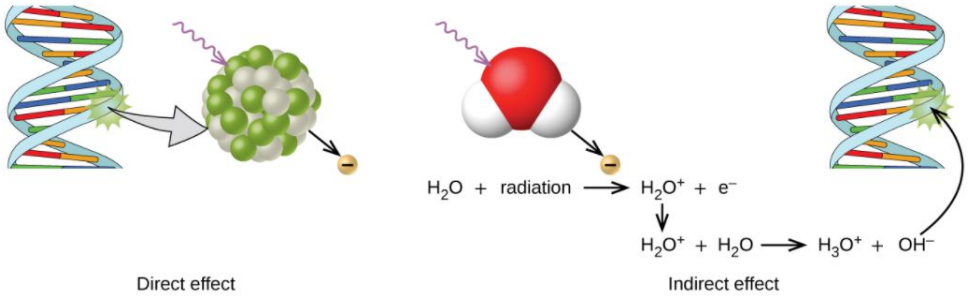

Figure 2.9: Direct and indirect damage examples (taken from [37])

2.9 Radiation Exposure and Dose

Radiation dosage amounts and units are naturally more complicated than those used in toxicology and pharmacology, and this complexity has grown as a result of various adjustments necessitated by growing radiation dosimetry principles. The Roentgen was the first commonly used physical quantity of radiation, which measured the ability of X-ray or gamma radiation to ionize air (R). Photons with an energy of less than 2.5 MeV were used to restrict exposure.

The pathways by which radionuclides are carried to members of the public serve as a starting point for calculating individual doses and evaluating health risks. Below are three main sources of radiation exposure that must be taken into account upon estimation of the dose to members of the public.

- External exposure due to submersion in contaminated air or due to radiation from an overhead plume or from radionuclides deposited on the ground,
- Inhalation of radionuclide-contaminated air, and
- Ingestion of radionuclides in water and foodstuffs.

A number of specialized quantities are employed in the assessment of radiation protection. UNSCEAR Report of 1988 [48] included the historical evaluation of the radiation quantities employed by the Committee. The International Commission on Radiation Units and Measurements approved a system of radiation quantities and units, and the International Commission on Radiological Protection (ICRP) [49] recommended new nomenclature and definitions.

2.9.1 Absorbed dose

Radiation dose can refer to a variety of things (such as absorbed dose, dose equivalent, or effective dose equivalent). The absorbed dose, D, averaged throughout a tissue or organ is the main dosimetric quantity utilized; its unit is joule per kilogram. The weighted dose quantities describe the link between this quantity and the risk of biological effect. ICRP has recommended weighting factor values for various types and energy of radiation incident on the body or emitted from within the body, as well as for specified tissues and organs. The averaged absorbed dose in tissue or organ T, modulated by the radiation weighting factor, W_R, is the quivalent dose, H_T.

2.9.2 Effective dose

The effective dose is determined for the entire body. It involves adding equivalent doses to all organs, with each dose modified to account for the organ's sensitivity to radiation. mSv are the units of measurement for effective dosage. Because different organs have varying levels of sensitivity to radiation, even though the equivalent dose is the same, the effective dose is the sum of equivalent dose to the organ times the appropriate tissue weighting factor for all organs. The effective dose is determined in sieverts (Sv) or mSv. In radiological protection, this is the most commonly utilized dose. A "dose" in Sv or mSv is the effective dose unless a specific organ is mentioned. The effective dose, H_T, is given by Eq. (2.37) below.

$$H_T = \sum W_R D_T, R \tag{2.36}$$

where W_R is the radiation weighting factor and DT_R is the average absorbed dose to tissue T due to radiation type R. The radiation weighted dose and the effective dose play an important role in radiological protection. The tissue weighting factors and the radiation weighting factors are presented in ICRP 103 [49]. The effective dose, E, is calculated using the Eq. (2.38), as described in ICRP publication 60.

$$E = \sum W_T \sum W_R D_T, R \tag{2.37}$$

In this study, the total effective dose for uranium isotopes were determined using the Eq. (2.39). The dose was assessed for all the age groups as will be discussed in chapter 4.

$$D_i(x) = \Sigma_p A_i p C_p(x) DCF_i(x) \tag{2.38}$$

where, $D_i(x)$ is the annual dose to an individual from age group x (Sv/a)
$A_i(p)$ is the activity concentration of nuclide i in product p (Bq/l)
$C_p(x)$ consumption rate of product p for individuals of age group x *(l/a)*
$DCF_i(x)$ is the dose coefficient for ingestion of nuclide i and age group x *(Sv/Bq)*

2.10 Excess lifetime cancer risk

Uranium is a radionuclide which is known for both its chemical and radiological toxicity [50]. It has been established that high concentrations of uranium greater than 15 μg/l in domestic water may present harmful biological effects in humans [2]. The assessment of radiological and chemical toxicity is critical. The Excess Lifetime Cancer Risk (ELCR) is assessed for radiological toxicity, while the hazard quotient is calculated for chemical toxicity.

Exposure to radiation over a long period of time is thought to increase the chance of cancer, therefore everyone is at risk of developing cancer. Excess lifetime cancer risk is an increased risk that a person may have of getting cancer disease as a result of long-term exposure to cancer-causing chemicals, this is according to Ref. [51]. ELCR was determined using the following equation based on calculated values of annual effective dose [52];

$$ELCR = E_(in) \times LE \times RF, \tag{2.39}$$

where, $E_(in)$ is the annual effective dose, LE life expectancy (year) 70/15 years and RF is a fatal risk factor per Sievert which is 0.05 as per the ICRP 60.

Chapter 3

Experimental Methods

3.1 Study Area

There are several methods used for uranium separation from different sample matrices. Some of the methods used are based on organic solvent extraction and other methods use anion exchange resin to separate uranium isotopes. In the present work, the latter method was used for uranium separation. This chapter describes the method and radioanalytical technique used for the detection of uranium isotopes in water samples collected in the West-Rand Area of Johannesburg in the Gauteng Province. The analysis for this study was carried out by counting on an Alpha Spectroscopy system with Passivated Implanted Planar Silicon (PIPS) detector, with the relative efficiency of approximately 12 %.

The study was carried out in West-Rand area which is part of Witwatersrand that was functionally merged with the Johannesburg conurbation in 1886. Figure 3.2 shows the location of the districts with the uranium mines in the West Rand Area.

According to the West Rand District Municipality integrated development plan, West Rand had an estimated population of 840 913 in 2016 as compared to 770 650 in 2006 with a growth rate of 9.1 % Figure 3.2 shows the population pyramid for the West Rand District between 2006 and 2016 as expounded by the StatsSA during the national census count.

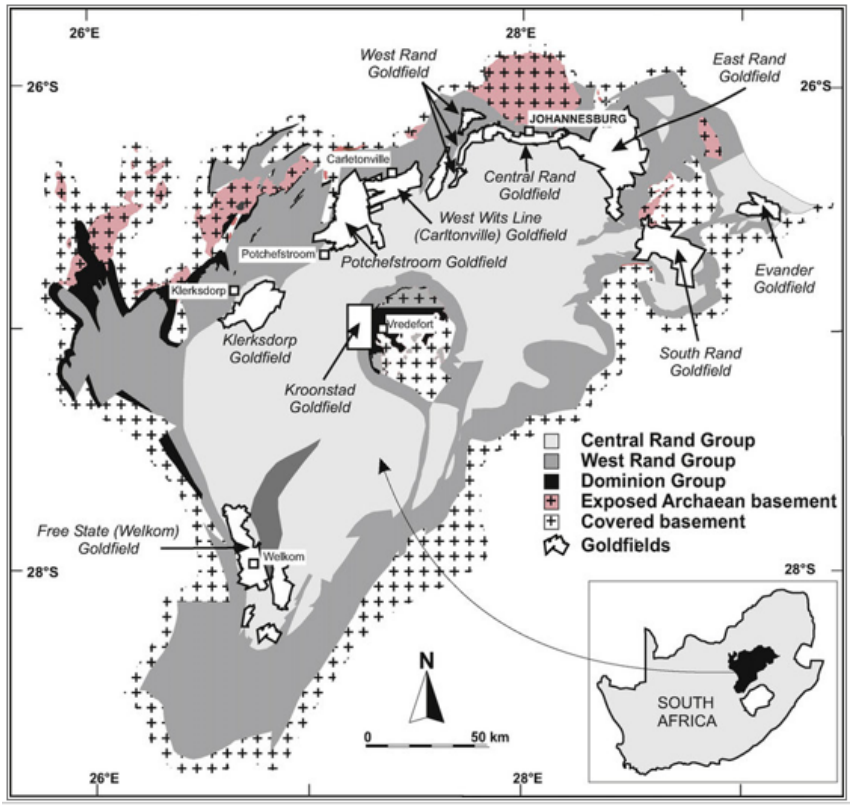

Figure 3.1: Geological map showing West Rand Goldfield where the current investigation was conducted (taken from Ref.[53])

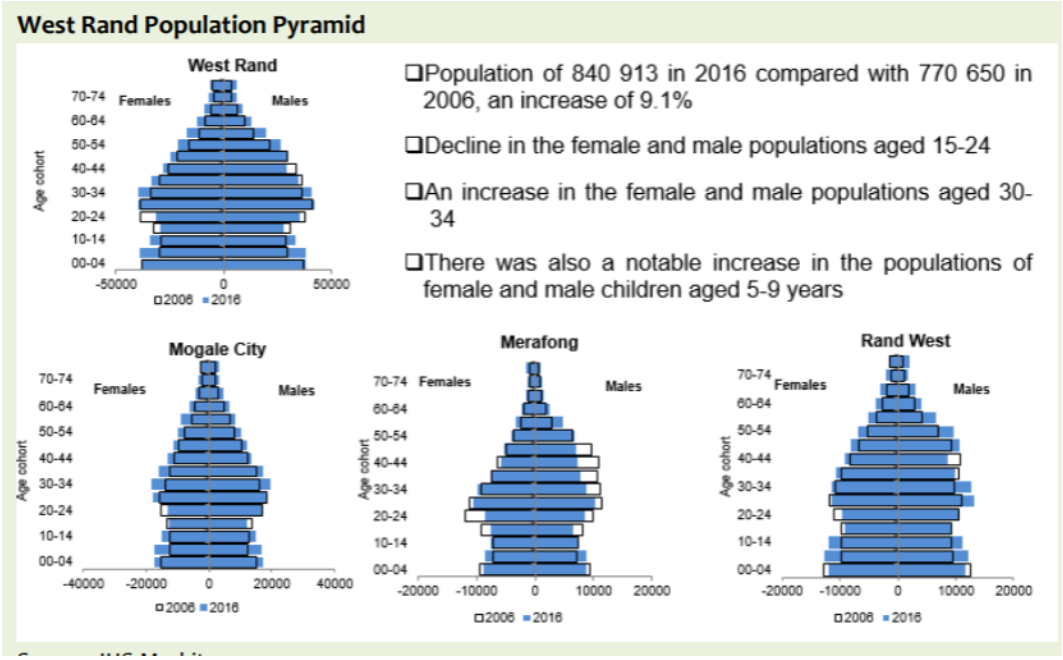

Figure 3.2: the population pyramid for the West Rand District (taken from Ref. [54])

There are several shafts systems, mine dumps and tailings dams that have been accumulated throughout the operation history of the mines in the area. The mining areas are within 13 km of the mine dwellings. The mine company owns and manages extraction and processing facilities where gold-bearing ore is treated.

The worker population in the study area is around 1700 meters and there are also some informal settlements within the mining area whereas located on farm land around the Carletonville area. The municipalities experience typical Highveld climate conditions that are warm and temperate, when compared to winter. The summers have fairly much more rainfall with high possibilities of thunderstorms, lighting and recently hail storm with the mean average rainfall of approximately 660 mm (November to March). The evenings and nights are relatively calm, and the temperatures have an average of 30°C (86°F) with clear skies and light winds. In winter season (June to August), rainfall is minimal with an average between one day and three days across the winter season. It is sunny in winter, with the sun shining for an average of nine hours per day and with the average temperature of 14°C. The spring and autumn seasons are mildly hot and sunny throughout with relatively high rainfall and temperatures. There are warm days and cold nights and occasional rain accompanied by light thunderstorms [55].

3.2 Materials and Methods

3.2.1 Sample collection and treatment

In the present work, a representative of water samples were collected from different sampling locations. Water samples collected upstream were pumped from underground into the environment. The selection of samples and sampling location was based on their accessibility to the mine proximity. A total of 44 water samples were collected during the winter and spring (also called dry season) and the other samples were collected in summer and autumn (called wet season). This was done in order to observe seasonal variation and to evaluate the effect of climate in the Uranium activities detected in the samples. The sample information is summarized in Table 3.1 below. Two litres of water samples were collected at site as per the standard sampling protocols and methodologies and WHO guidelines, using pre-cleaned polyethene containers,

which were labelled accordingly with marker for easy identification. Figure 3.3 shows a picture taken during sample collection activities at West Rand after sampling area identification.

Table 3.1: Origin and sample information of the samples under investigation

Sample matrix	**Water**	**Sample detail**
Sample No.	**Sample Area**	**Description of sample area**
A1	Blyvooruitzich (Bly4)	Shaft4 discharge point
A2	Blyvooruitzich (Bly6)	Shaft6 discharge point
A3	Blyvooruitzich comb	Combined water downstream from all operations
A4	Driefontein	Downstream of Gold mining operations
A5	Driefontein	Settling ponds
A6	Driefontein	Water from discharged area
A7	Kloof 10	Water from shaft 10
A8	Kloof down	Downstream of operations
A9	Ezulwini-inlet	Peter Wright Inlet
A10	Ezulwini	Peter Wright Outlet
A11	Driefontein	Drinking water from water treatment facility nearby



Figure 3.3: A picture taken during water sampling activities

The collected samples were each packed and stored in a cooler box container and transported to the National Nuclear Regulator radio-analytical laboratory. All the sample information were recorded appropriately and samples assessed for quality and adequate volume for testing prior to receipt by the laboratory. The samples were received, surveyed, logged in and assigned a unique identification number for sample tracking by the laboratory personnel. The surveys were done to check for any contamination prior to acceptance by the laboratory, while the screening was done using a calibrated contaminated monitor as shown in Fig. 3.4 below. The samples were stored at room temperature in a designated sample processing area with numbered shelves for easy identification as illustrated in Figure 3.5.



Figure 3.4: Picture taken of the contamination monitor used with its calibration certificate



Figure 3.5: Prepared water sample designate storage area

The sample storage areas are designed to prevent contamination, cross contamination, or damage to the sample packaging and any seals. The samples were acidified with Nitric acid to pH2 to terminate the biological activity, stabilize the samples and also to prevent the radionuclides from sorbing to the

container wall surface. Samples awaiting analyses are in designated storage location to protect the integrity of the sample.

3.2.2 Sample preparation

Preparation of water samples may seem to be mostly routine aspect of the Laboratory protocol. Nevertheless, preparing the sample for analysis is of utmost importance because the quality of the measurement depends upon the quality of the preparation. The results of this test may be flawed if the aliquot used for testing is not representative of the original sample. An error in sampling and sample preparation is usually greater than an error in a methodology itself [30]. The samples are prepared to convert field samples into laboratory sample suitable for the analytical method to be applied. The collected water samples were filtered and acidified with nitric acid to pH2 immediately after arrival at the laboratory and not in the field as prescribed in literature in Ref [30]. Adding acid to unfiltered sample may leach radionuclides from non-dissolved matter thereby increasing the radioactivity concentration of the water sample. Acidification immediately after collection (on the field) is a common practice in order to prevent absorption of trace elements onto the container [56].

Before filtration, preliminary measurement of conductivity and turbidity in the sample can be conducted in order to provide more information about the collected field sample. The results especially of the turbidity is helpful in deciding the appropriate sample volume for the radiochemical separation and analysis. Total Dissolved Solids (TDS) value of less than 25 mg.L^{-1} is for the surface water and 1 mg.L^{-1} rainwater, whereas a range of 95 - 1100 mg.L^{-1} can be expected for water in contact with sedimentary rock formations. According to Ref [57], the acceptable Total Dissolved Solids limits for drinking water is 1200 mg.L^{-1} . When there is no previous historical information from the sample collecting area, the measurements are extremely relevant. Preliminary conductivity measurements requires little to no sample preparation and are carried out on a separate section of the sample to avoid cross contamination and radionuclide loss due to equipment interaction. The water samples used in this study were filtered using both a 0.8 µm and a 0.45 µm membrane filter, filtration equipment is shown in Fig. 3.6 below. A measure of maximum 200 ml of the filtered sample was used into a 400 ml glass beaker. Uranium-232 tracer working solution (100 mBq/g) was also added. The sample was evaporated by using a hot plate on a fume hood to a volume of 10 to 50 ml.

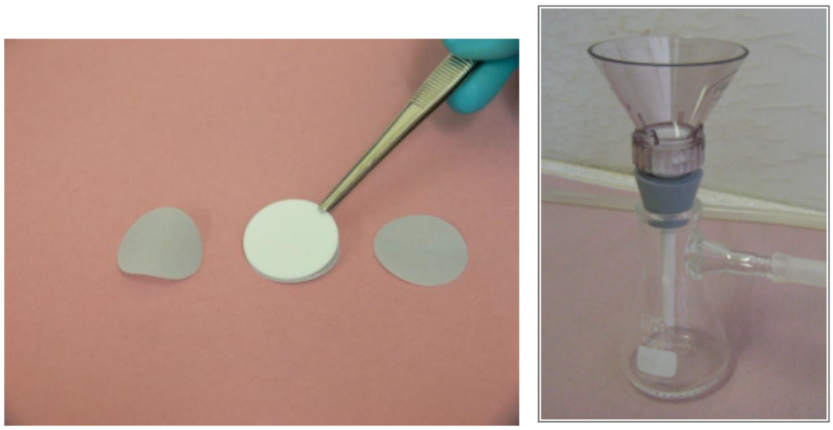

Figure 3.6: LHS: Typical micro-precipitate deposited by filtration with radionuclide (s)on a fine porous size membrane filter paper
RHS: Prepared filtration funnel with 0.1 µm polypropylene and 25 mm in diameter

3.2.3 Alpha source preparation methods

To avoid poor energy resolution defined by numerous peaks and to generate a homogeneous sample for measurement, a variety of procedures are routinely utilized for test source preparation. According to Ref. [58], the main aim for source preparation is to prepare a thin, homogeneous, flat and stable source suitable for counting in any detector. This suggests two sample preparation requirements: first, a thin sample must be produced, then chemical separation must be performed to avoid chemical or radiochemical interferences. To guarantee an accurate quantitative analysis as well as high resolution, appropriate sample preparation is required. The two methods commonly used for source preparation include electrodeposition, Precipitation and Co-precipitation [30]. All of these methods are aimed at achieving the smallest feasible surface thickness. Each method depends on a specific separation mechanism, resulting in different filter or metal disk mounting strategies (substrate).

3.2.3.1 Electrodeposition method for source preparation

Radionuclides of interest are electrodeposited on a suitable metallic surface, the voltage is applied between the two electrodes by using a DC generator as shown in Fig. 3.7. This will result in the reduction of the metal cations dissolved in the electrolytes. The reduction that take place at the cathode leads to the formation of a deposit of actinides in hydroxide form. A thin stainless steel disc,

a platinum disc, or a metal-coated plastic film is commonly used as the cathode upon which radionuclide accumulates [58]. The platinum wire stirring rod was used as the anode of the cell. Electrodeposition of radionuclides from a solution generally results in flat, homogenous test sources with slightly improved energy resolution. Thus, this technique is very appropriate for preparing sources of alpha emitters, especially the actinides, which include uranium, plutonium, thorium, americium, and neptunium. For some of the long-lived radionuclides, such as ^{232}Th, there may be micrograms of the plated nuclide that can affect the alpha spectrometry resolution. Several shortcomings are listed below for the electrodeposition techniques for source preparation [59]:

- Interferences within the electrolyte solution or any interferences resulting from an incomplete separation prior to source preparation may potentially be deposited onto the planchet. Increasing mass onto the planchet results in an increasing potential for attenuation.
- For the electrodeposition, the samples cannot be massive, typically less than 100 nm, because a thick deposition layer will accumulate onto the planchet.
- Stainless-steel planchets corrodes due to electrolytic solution and platinum planchets is preferred but it's expensive.
- Planchet can be re-used but time consuming and probability of cross contamination can also increase if the planchet is not cleaned properly.
- The apparatus of electrodeposition is difficult to maintain and can have many challenges with the overall set up.
- One of the most common issues is leakage of cells that may cause a loss in sample and contamination onto the apparatus.
- Other challenges that may occur are current fluctuations and pH changes during electroplating which can lead to low isotope recovery

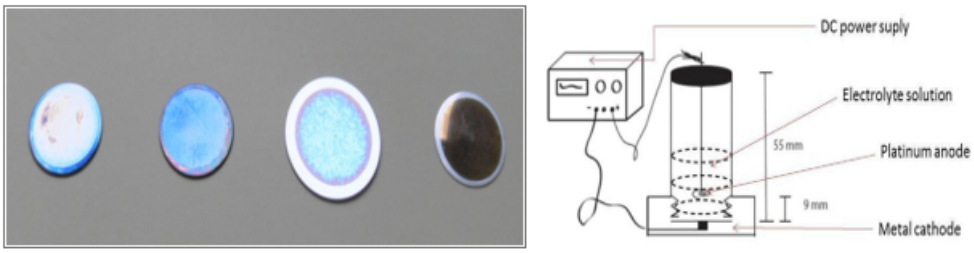

Figure 3.7: LHS: Source prepared on a stainless steel disc
RHS: Schematic diagram of the electrodeposition cell (taken from Ref.[60])

3.2.3.2 Precipitation and co-precipitation

By producing an insoluble substance, precipitation is used to isolate and collect a specific radionuclide from other (foreign) ions in solution [30]. Either the radionuclide is precipitated from solution itself, or the foreign ions are precipitated, leaving the radionuclide in solution. Sometimes a radionuclide is present in solution at sub-micro concentrations, i.e., levels so low that the radionuclide will not form an insoluble compound upon addition of a counter-ion. In these cases, the radionuclide can often be brought down from solution by co-precipitation, associating it with an insoluble substance that precipitates from solution into the filter paper as shown in Fig. 3.6. This phenomenon is especially important in gravimetric analysis and radiochemistry.

The approach utilized in this study allows nuclides of interest to be co-precipitated as hydroxide or fluoride utilizing cerium or neodymium fluoride. Some of the advantages of this method include good resolution provided the sample layer mass is kept below 100μg, highly selective and virtually quantitative, convenient, simple process and high degree of concentration is possible. This method has some drawback such as contaminated precipitate by carrying of ions or post-precipitation and co-precipitating agent might contain isotopic impurities of the analyte radionuclide. The use of improved filters and detectors (such as silicon implanted detectors) can yield a resolution of 40 to 50 keV [61].

3.2.4 Alpha source preparation used for present study

Uranium isotopes are separated by Eichrom TEtraValents Actinides (UTEVA) resins prior to measurement by alpha spectrometry. The extractant in the UTEVA Resin from EiChrom Inc., diamyl, amylphosphonate, extracts nitrato complexes of the actinide elements. The formation of these complexes is driven by the concentration of nitrate in the sample solution. The UTEVA resin has the specificity to hold actinides with oxidation states of greater than or equal to IV, and to have a low affinity for actinides and elements with the oxidation states of less than or equal to III [62]. During the chemical separation, the oxidation states of some radionuclides change to allow the simultaneous extraction of natural and anthropogenic radionuclides. A calcium phosphate precipitation was used to concentrate actinides from water samples. In what follows, a radioactive tracer was added to monitor chemical recoveries and correct results to improve precision and accuracy. Uranium-232 standard solution was used as a tracer with a specific activity concentration of approximately 1.0 mBq/ml added to the sample. A blank analysis was also performed with tracer as a potential way to identify any presence of uranium isotope analytes in the tracer.

Radionuclides such as ^{241}Am and ^{238}Pu, ^{237}Np and ^{234}U, or ^{210}Po and ^{232}U with unresolvable alpha energies were chemically separated from the samples to enable measurement. High levels of phosphate in the sample may cause reduced recoveries of actinides during calcium phosphate precipitation and column separations. Adjusting the amount of phosphate added to co-precipitate the actinides may be necessary in such cases. The sample preparation method used adequately recovers actinides from freshly collected, well preserved, homogenous water samples.

The uranium isotopes are then separated from the water by chemical separation steps involving resins and chromatography; after which the uranium is co-precipitated on a filter paper for counting on the alpha spectrometer. Stages and methods involved from sample preparation are illustrated in Figure 3.9. This technique is faster and more reliable than those involving electrodeposition and gives consistently higher yields. The method is more rapid, more economical, and more efficient and yields better decontamination factors, high recoveries, and excellent resolution of the alpha spectra for uranium, plutonium, americium, and thorium. It has been observed that the recoveries

are higher than 90%. This method is convenient for routine analysis and for the determination of low activities and short lived radionuclides. Decreasing of resolution (40-70) keV and high sensitivity on impurities are some of the shortcomings [63].

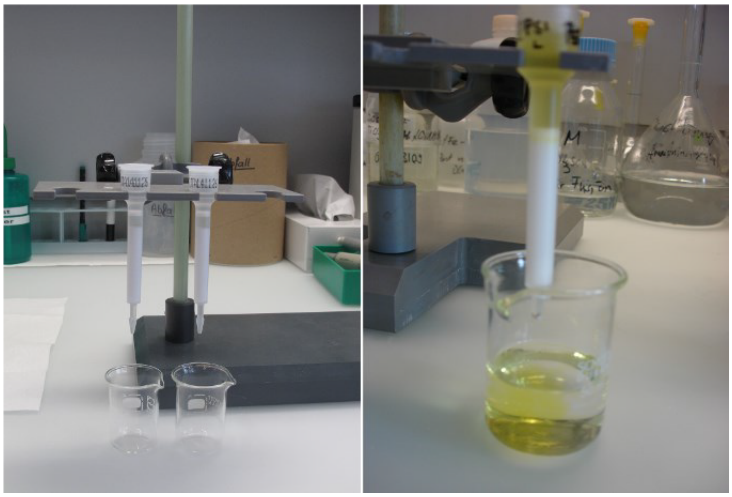

Figure 3.8: Pictorial representation of chemical separation set-up using UTEVA resin

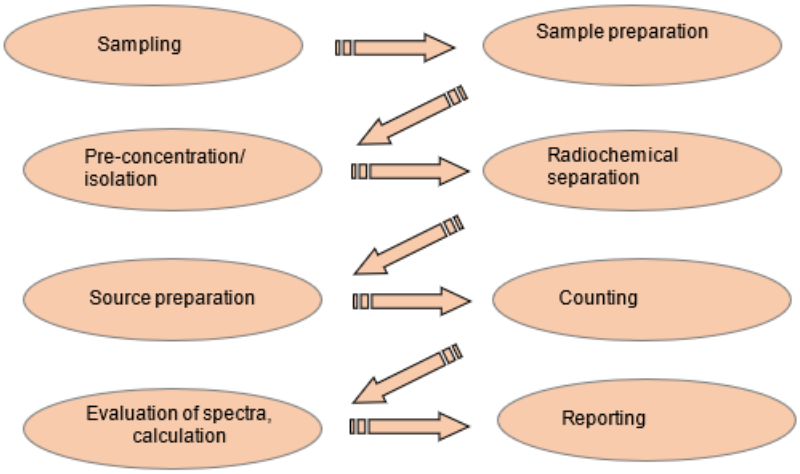

Figure 3.9: Schematic diagram illustrating stages of methods involved in uranium sample preparation for alpha spectrometer measurements

For low uncertainty (typically below 5%) on the results, electrodeposition might be used for very low activity samples as the co-precipitation method (directly on filter paper) can result in a thick precipitate on the filter paper resulting in higher uncertainties due to self-absorption. Thicker precipitate also leads to spectra resolution degradation [64].

A thin, flat and uniform uranium source is prepared by co-precipitation for the high-resolution alpha spectrometry, which allows adequate transmission of the alpha-particles to the surface of the detector. The source must be as thin as possible and homogeneously distributed on a flat smooth filter paper or aluminium disc in order to minimise energy loss in the source and to detect the emitted alpha-particles with optimum energy resolution.

3.2.4.1 Tracers

The ^{232}U solution (70,6 ± 1,1 years) was used as a tracer in order to calculate the chemical yield, this is attributed to the fact that it has similar activities as those of uranium isotopes to be measured. Daughter progeny radionuclides (^{228}Th and ^{224}Ra) grow in from ^{232}U, and may interfere with other analytes. Thorium may recoil into the detector from decay of ^{232}U, and the background for each detector should be monitored for this potential source of interference. The working solution of approximately 100.0 mBq/ml was prepared by the dilution of a standard solution that has traceability to national and international standards. 200ml of samples were spiked with ^{232}U tracer, and concentrated by evaporation. The tracer contained 0.8% impurities of Thorium-228.

3.3 Measurements Techniques

Alpha spectrometer and ICP-MS (Inductively coupled plasma mass spectrometry) are analytical techniques used in this study. Alpha Spectrometry was used to determine the activity concentration of the three main uranium isotopes and ICP-MS was used to quantify ^{208}Pb, ^{209}Bi, ^{232}Th for a selected number of samples. Alpha spectrometer is highly applied, due to its high energy resolution, excellent stability, cost and intrinsically low background (as a result of which there is a high sensitivity) [65]. One of the main drawbacks for alpha spectrometry, is that it is very time consuming and cannot resolve peaks with similar energies.

The high resolution is ensured by the thin entrance window over the detector surface. It reduces energy straggling in the entrance window, due to the random nature of the interaction of a charged particle with the detector material. This leads to a spread in energy if a beam of charged particle passes through a certain thickness of absorber and, consequently, results in an increase in the peak width. The detector's sensitivity is boosted by its high resolution, which lowers the background below the peak. A depletion depth of 140 µm is sufficient to absorb alpha particles with energies of up to 15 MeV, encompassing the entire range of alpha producing radionuclides. [29].

The principle of the Alpha spectrometry involves the recording of the energy of the emitted alpha particles in the form of a pulse height distribution. The pulses are created in a sensitive part of the detector volume which can be gaseous, liquid or solid, and registered after electronic amplification. Although the alpha radiation exhibits discrete energies the interaction between alpha particle and detector is subjected to counting statistical variations which cause the emergence of a broadened peak instead of a discrete line. Commonly used alpha detector types are ionization chambers, proportional counters, solid-state (silicon), semi-conductors and scintillation counters (plastic, ZnS phosphor-photomultiplier tube combination, or a liquid organic cocktail) [66].

According to the IAEA's analytical quality in Nuclear Application Series No. 19 [67], an alpha particle spectrometer can be evaluated by several parameters such as the type of the detector, performance of the detectors, the quality of the calibration source, and the source to detector geometry all influence the counting efficiency, the intrinsic background, and thus the detection limit, the possible contamination and the quality of the measured spectra, including energy resolution and peak tailing [68].

Typical heavy element alpha decay energy falls within the region 4 to 9 MeV because of short range of alpha particles. The strong interactions among alpha particles and air components cause a significant energy loss which complicates spectral analysis. Thus, the measurements are carried out under vacuum in the case of solid detector types (i.e. scintillator crystals, semi-conductors). Further optimization is achieved by adequate arrangement of source and de-

tector to each other [69].

Below are the few factors influencing the resolution and the efficiency of the detector as highlighted by Ref. [56].

- Detector to source distance: All the alpha particles reaching the sensitive or active area of the detector will be counted. The counting efficiency is given by geometric efficiency, $\eta = \frac{\Omega}{4}\ \pi$, where Ω is the solid angle under which the detector subtends the source. For case of a circular detector Ref. [56] indicated that on the axis with a circular isotropic source disk, the solid angel can be computed by general purpose Monte Carlo radiation transport algorithm MCNP [29]. The solid angle is widely used during absolute methods to calibrate detectors or to determine (using absolute methods) the activity of a radioactive source. The solid angle is the fraction of source particles that interacts with the detector aperture and so it is not purely geometric—the angular distribution of the source is also a factor [70].

- Source radius: The efficiency of the bigger detector is much greater, depending on the source radius used. The diameter of the detector should be greater than the diameter of the source. If a uniform source with known activity, the total number of counts registered is proportional not only to the efficiency but also the total activity of the source deposited on the sensitive surface area.

- Source thickness: Activity measurements of alpha particle with a thickness precipitate will require self-absorption correction

  Thus, the source must be uniform, homogenous distributed, stable, very thin and flat (nearly massless source mount) to allows adequate transmission of the alpha particles to the detector surface and to avoid energy straggling due to self- absorption. Self-absorption is directly proportional to the thickness of the sources and inversely proportional to the specific activity concentration. For typical specific activity values of 100 Bq/cm, the self-absorption is insignificant for carrier-free source. The effect of thickness of carrier-free source depends on the transition probability of the radionuclides of interest, which increases with high life, e,g ^{238}U.

By using this technique, a wide variety of alpha emitting nuclides with long half-lives can be determined with respect to the time required to prepare the

sample. Beta-emitting radionuclides can also be determined indirectly, if they have alpha emitting progeny which may be measured on the source following a suitable in growth period in order to reach equilibrium. In high-resolution spectroscopy, a sample is chemically processed and electroplated, which is followed by in-vacuum measurements with Si detectors. This procedure provides excellent radionuclide identification and determination; however, it is labor intensive and time consuming. Alpha Spectrometry is highly sensitive, with low detection limit of about 1 mBq per litre [56]. The draw back about this technique is the initial cost for the procurement of the Alpha Spectroscopy system and also the method is labor intensive.

Because of the low level of detection limits which can be attained, high and good selectivity, and acceptable precision and accuracy, inductively coupled plasma–mass spectrometry is one of the most significant techniques for elemental analysis [71]. It enables element analysis at concentrations as low as 1 part per trillion (ppt) or even lower. Although some laboratories continue to use older techniques such as atomic absorption spectroscopy and atomic emission, there has been a progressive shift toward ICP-MS in recent years, notably in the last decade [72]. The ability to do isotope determination, as well as isotope ratio and dilution analysis, is one advantage of ICP-MS for inorganic elemental analysis. The principle involves ionizing the material in an inductively coupled plasma (ICP), then extracting the ions and separating and quantifying them in a mass spectrometer. Quadrupole, sector field mass spectrometry (ICP-SFMS), and multi-collector (MC) ICP-MS devices are among the mass spectrometers that can be used with an ICP source. These are sector field instruments with numerous detectors (often Faraday cups) for simultaneous detection of ions of various masses.

3.3.1 Alpha Spectrometry system

Alpha-particle spectrometry is an important and useful radio-analytical technique used for the qualitative, quantitative, identification and determination of α-emitting radionuclides in environmental, biological and nuclear technology related samples [69]. Alpha Spectrometry together with radiochemical separation allows the determination of low activity concentration of many radionuclides including uranium isotopes.

The alpha spectrometer used in this study was an integrated multi-detector and multi-channel analyzer (MCA) based on 12-chambers. Each incorporated

channel is an independent alpha spectrometry system with high performance ion-implanted silicon charged-particle detector located in its own measuring chamber. Furthermore, the electronics of the system consist of a variable detector bias supply, a preamplifier, a shaping amplifier with adjustable gain, a pulse stretcher and bias amplifier. All the 12-chambers are connected to an integral vacuum manifold with a single connector, with the vacuum pressure range set at 12 mbar as shown in Fig. 3.10. In order to obtain the best alpha peak resolution, the PIPS detector is operated in a near vacuum condition. This is done in order to eliminate the alpha-particle energy degradation from interactions with air molecules prior to striking the detector face. Measurements of alpha particles rely on the interaction of alpha-particles with the detecting medium. This interaction creates a charge, which is amplified and output as a voltage pulse proportional to the deposited energy of the incoming alpha particle [73]. The electric pulse from the detector is analyzed by the electronic systems. Data analysis software provides a spectrum, in which the number of pulses (counts) recorded in each energy interval is shown. The analysis of the count rates in the uranium isotopes alpha-energy windows allows the determination of the test sample activity concentration for ^{232}U, ^{235}U and ^{234}U, after correcting for the blank count rate, volume of the test sample and chemical yield. The chemical yield is determined by measuring the net count rate of uranium-232, added as a chemical yield tracer.

Alpha spectra of the samples were measured with a Canberra Alpha Analyst spectrometer shown in Fig. 3.11 using Apex Alpha Software. The instrument is equipped with a Passivated Implanted Planar Silicon (PIPS detector) semiconductor detector (sensitive area of 450 mm^2). Figure. 3.12 shows the PIPS detector used for alpha spectra analysis and quantification. The counting times was 24 hours as per the standard laboratory procedure.



Figure 3.10: Alpha Spectroscopy Vacuum pump



Figure 3.11: Alpha Spectroscopy from Canberra with 12 chambers

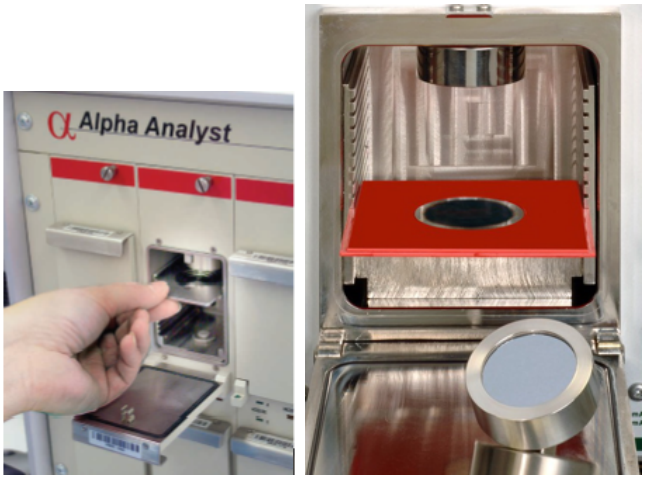

Figure 3.12: Canberra Alpha Analyst spectrometer situated at NNR Environmental Laboratory

3.3.2 Calibration of Alpha Spectrometer

The measurement of Uranium isotopes was conducted by using an alpha spectrometer in order to identify, quantify and determine the activity radionuclides of interest based on the alpha particles emitted in the decay process. The measurement for this study was taken using the calibrated detector for both energy and efficiency calibration. A multi-nuclide radioactive reference source was used to calibrate alpha detectors using a direct count method. The efficiency measurement of the alpha spectroscopy used in the NNR Environmental laboratory must be known in order to determine the chemical recovery for the measured sample. The reference source have the following properties:

- Product Code: MIX-EAB24U-7Bq
- Certificate of Calibration 92047 (Eckert and Ziegler Analytics)
- 24.1 mm diameter x 0.65 mm thick stainless steel disk



Figure 3.13: The standard radionuclide source prepared by electrodeposition onto a stainless steel disk

3.3.2.1 Energy Calibration

The energy calibration of the alpha system was done by counting a certified reference source obtained from Eckert and Ziegler Analytics. The calibration of the alpha spectrometer was performed for each chamber. This was done by using an alpha standard electro-deposited onto a stainless steel disc sources of mixed radionuclides as depicted in Fig. 3.13. The source contains ^{238}U, ^{234}U, ^{230}Pu and ^{241}Am radionuclides with the energy range from 4.18 to 5.47 MeV as shown in Table 3.2. The radioactivity concentrations and their associated uncertainties for these radionuclides are also included in Table 3.2.

The calibration sources were counted for 1800 seconds of livetime to produce a well defined peaks, where the channel number of the photo-peak is proportional to the energy of each radionuclide. The uncertainty of the activity concentrations was 3% at the 95% confidence level. The energy calibration of the Alpha Spectrometer was performed and the energy resolution of the detector was determined by calculating the photopeaks full width at half maximum (FWHM) [74]. A plot of energy calibration curve for the source is shown in the Fig. 3.14. This provides a linear relationship between the energy and the channel number.

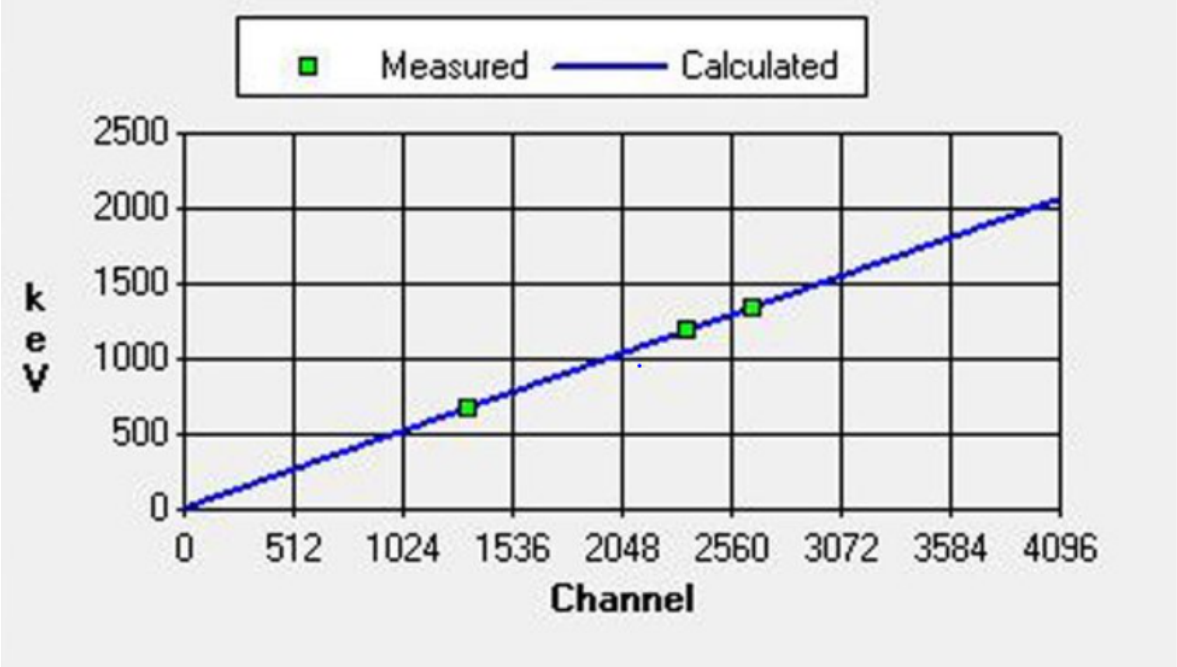

Figure 3.14: Energy calibration curve for the standard source for the PIPS detector

Table 3.2: Calibration source with corresponding activity concentrations and photo-peak energies

Isotope	Energy (Mev)	Activity concentration (Bq)	Uncertainty (%)	Channel number
U-238	4.184	1.551	3	244
U-234	4.497	1.497	2.6	328
Pu- 239	5.148	1.463	3	284
Am-241	5.479	1.526	3	433

3.3.2.2 Efficiency Calibration

The counting efficiency is the relationship between the activity concentration of the nuclide in the count sample and the area of the corresponding photo peak in the pulse height spectrum, i.e. fraction of the particles reaching the sensitive area of the detector (entrance window). The counting efficiency was determined by measuring the peak area expressed as a count rate (Nc) of a calibration source. This was done with known activity (A) and its associated

photon yield (Y), and then calculate the efficiency (= ε) using Eq. (3.1) the below.

$$\varepsilon = \frac{Nc}{YA} \tag{3.1}$$

The efficiency values were determined by dividing the resultant net count rate (cps) by the alpha emission rate of the source as illustrated in Table 3.3. The region of interest (ROI) was between channel 600 and 1935 of the pulse height spectra acquired for 1800 s with multi-channel analyser of 4096 channels.

Table 3.3: Counting efficiency using the calibration source

Isotope	Net counts	efficiency	Activity concentration (Bq)
U-238	700	0.139	1.551
U-234	694	0.136	1.497
Pu- 239	689	0.135	1.463
Am-241	663	0.210	1.526

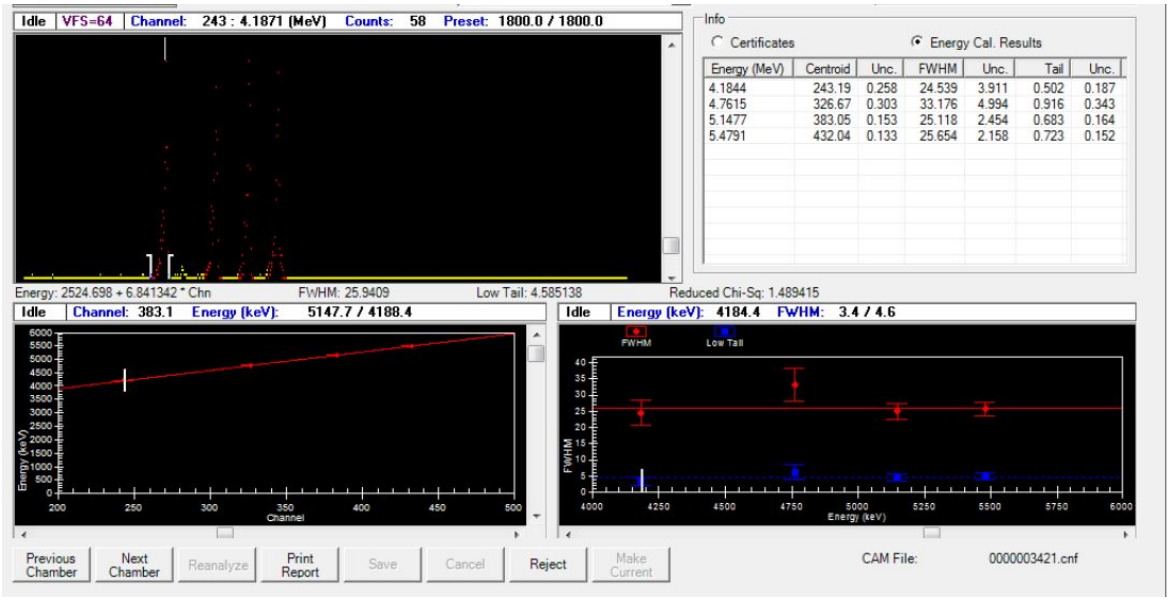

Figure 3.15: Picture illustrating the Energy efficiency on the Alpha Spectrometer

3.3.2.3 Quality assurance

In order to ensure the quality of the test results, quality performance checks are done on the Alpha Spectrometry systems maintained at the NNR Laboratory. A performance test was done in order to check the detector efficiency, this was carried out by using the ^{241}Am source which was also used to check for low-energy tailing. In order to check the resolution of the peaks the pulsar test is also performed. The width of the pulsar peak (FWHM) at 5 MeV was also monitored to detect any degradation in the detector. The energy of the peak was monitored to detect any energy shifts in the detector electronics. The background count rates for the region of interest from 3 MeV to 9.4 MeV were used to check for contamination of the detector.

The system background of each detector was determined with an empty source support, and counted for 24 hours on shelf 3 (9 mm detector-source spacing) with approximately 12% detector efficiency. Shelf 3 was used for all the measurements of samples prepared at the laboratory. The energy calibration and energy resolution checks for each detector were done with reference calibration source. To monitor the quality of sample preparation the following quality assurance samples were prepared with each batch of unknown samples.

- Reagent blank
- Duplicate sample in a batch
- Laboratory control sample

3.3.3 ICP-MS measurements

The sample introduction system, inductively coupled plasma (ICP), interface, ion optics, mass analyzer, and detector are the six fundamental compartments of a single quadrupole ICP-MS. The instrument is depicted in Fig. 3.16 as a basic schematic. Liquid samples are nebulized in the sample introduction system, which produces a tiny aerosol that is then delivered to the argon plasma. The high-temperature plasma atomises and ionizes the material, producing ions that are extracted through the interface region and into the ion optics, which is a collection of electrostatic lenses. The quadrupole mass analyser's ion optics focuses and guides the ion stream. The mass analyser divides ions into groups based on their mass-charge ratio (m/z), which are then measured at the detector. Sample preparation for water sample requires dilution with

acids and water prior to analysis. In ICP-MS, a sample with a total dissolved solids (TDS) level of 2 g/L is commonly advised to reduce sample matrix effects and to prevent the nebuliser from clogging. For more detailed description of ICP-MS operations and measurement techniques see Ref. [75].

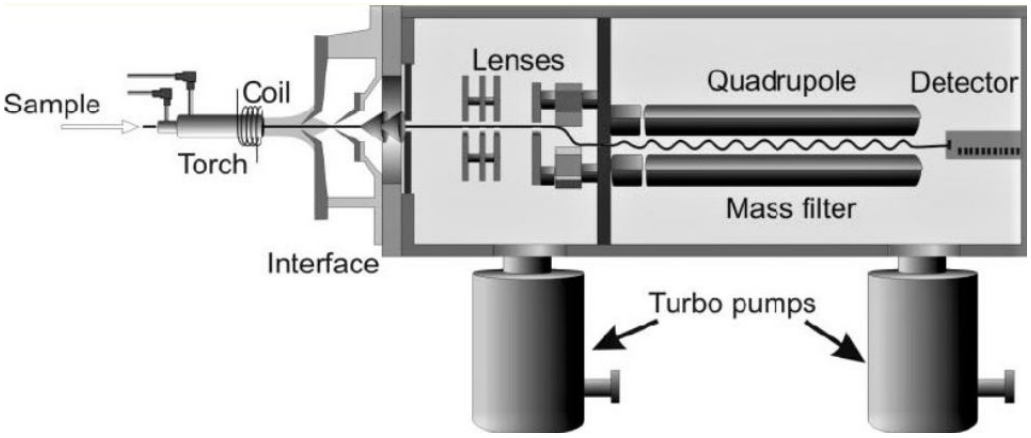

Figure 3.16: A schematic diagram of ICP-MS (taken from [71])

3.4 Detection systems

When radiation interacts with charged particles, the energy of radiation is passed on to the matter and the radiation is attenuated or even stopped. According to Ref [56], the atoms or molecules of matter are brought to a state of higher energy, an excited state, or they are ionized if the energy of the radiation is high enough. Alpha particles, beta particles and gamma rays are known as ionizing radiation. On passing through a gas, these radiations create positive ions and electrons by ionising the gas.

Those charged particles either cause chemical reactions or recombination, finally producing neutral specimens again. But if an electric field is applied, the positive ions start to migrate to the cathode and the electrons are attracted by the anode. If the field strength, the applied voltage per unit length, is high enough to prevent recombination during migration of ions and electrons, all of them arrive at the electrodes. They are collected at the electrodes, and by the detection of this electric charge using a suitable electric circuit, which gives an

indication of the presence of ionizing radiation.

Radiation detection systems come in many different types, but they are all based on the same fundamental principle of transfer of part or all of the radiation energy to the sensitive part of the detector material. The suitability of the detector systems for a given kind and energy of radiation depends on the type (pressure, composition) of filling gas to be ionized. Also environmental factors such as temperature should be recognized, the geometric design of a detector depends mainly on its application. The list below provides the most common detectors or detection systems that are commonly used, depending on the specific needs of the device [39]:

- Gas-Filled Detector
- Solid- Sate Detector
- Scintillation Detection systems
- Silicon and Germanium Detector system

The minimum energy (in electron volts) required for such ion pair formation in a given gas is called the ionization potential. This value differs markedly for different gases and is dependent on the type and energy of the charged particle. A more meaningful value is the average energy lost by the particle in producing one ion-pair, which is nearly independent of particle energy and type (and is about 35 eV). The rate of energy loss will depend on the energy and type of charged particle. Alpha particles will create ionization -10^{-4} – 10^{-5} ion pairs/cm of path length) whereas β particles will produce 10^{-2} -10^{-3} ion pairs/cm and the passage of γ rays will result in 1-10 ion pairs/cm [76].

3.4.1 Solid-sate Detector

The operating principle for solid-state detectors is similar to that of the gas-filled detector, except that collection at the electrodes of electrons and electron holes replaces electrons and positive ions [77]. Semiconductor materials can be used for the detection of charged particles, especially with low energy, such detectors are called solid-state counters. These types of detectors are solid-state ionization detector, having the following advantages over gas-filled detectors [78] :

- The energy required for the creation of an electron-ion pair is 3 eV as compared to 35 eV in a gas, which provides for stronger signal and better counting statistics.
- The stopping power is higher than in the gas filed detector due to the denser detector material. And thus becomes possible to stop in the detector material.
- Larger numbers of electron- ion pairs are formed yielding to better energy resolution.

3.4.2 Silicon and Germanium detectors

The introduction of semiconductor detectors for the measurement of radioactivity has substantially simplified and improved both charged particle and gamma-ray energy spectrum measurements. Solid-state detectors particularly silicon for alpha particles and germanium for gamma rays are mostly effective for spectral analysis. Spectral analysis is used to identify the radiation by its characteristic peak energy and to determine its activity concentration based on the count rate within the peak region of interest. The activity concentration of radionuclides of interest in the sample can be determined according the Eq. (3.2) [79].

$$A = \frac{1}{B.R.\gamma \times \eta\gamma \times t \times M} \times Ns\gamma \tag{3.2}$$

where,
A- is the activity concentration of radionuclide (i) in Bq/kg, or Bq/l
$B.R.\gamma$ - emission probability of the gamma line corresponding to the peak energy (γ)
$\eta\ \gamma$ - efficiency corresponding to the peak energy (γ) at the specific geometry,
$Ns\gamma$- net count under the peak area of the selected gamma line for the measured sample,
t- real counting time, and
M- mass of the sample (kg or mL)

Further advantages of restricting analysis to the narrow band of the characteristic energy peak are reducing interference from other radionuclides in the sample and from background radiation. The detection system for Alpha particle and gamma rays spectrometer differs. The gamma detector (crystals) are either p or n type and are grown with the low impurity level needed with

dimensions up to 10 to 12 cm. The detectors fabricated from these crystals are called instrinsic or high-purity germanium (HPGe) detectors. Germanium detector has a relatively low band gap of the characteristic energy peak, that reduces the interference from other radionuclides in the sample and from background radiation.

The detection systems require highly stable power supplies and amplifiers to support analysis at high-energy resolution. A typical gamma-ray spectrometry system is composed of a HPGe detector (usually semiconductor, or scintillator, for example NaI(Tl) or plastic scintillator) with lead shielding, for background reduction; high voltage power supply; electronics for signal processing (preamplifier, amplifier, multichannel analyzer); computer and dedicated software. The spectrometric system records, stores and processes the gamma-ray spectrum of the counted sample, using validated computer software packages such as Genie 2000. The detector has a cryostat for cooling during counting of samples. A Dewar flask that contains liquid nitrogen coolant is commonly used, but electromechanical cooling can be substituted.

For alpha particles, the solid-state detectors used are silicon diodes consisting of a very thin sensitive surface of p-type silicon over a much thicker wafer of n-type silicon. A reverse bias of about 50 V is applied across the diode from a stable power supply. Alpha particles striking the sensitive surface of the detector into the n-type layer and produce electron-hole pairs which are direct proportion to the energy of the alpha particle. The electron-hole pairs are accelerated to the electrodes and produce a pulse which is collected by a charge sensitive preamplifier. The pulse is amplified by a suitable low-noise amplifier and fed into a multichannel pulse height analyzer. The latter is simply a device for sorting the incoming pulses on the basis of their amplitude and storing them in appropriate bins or channels that are linearly related to the energy [80]. A schematic representation of an alpha spectrometry is shown in Fig (3.17), including high voltage supply unit, preamplifier, multichannel analyzer and data output.

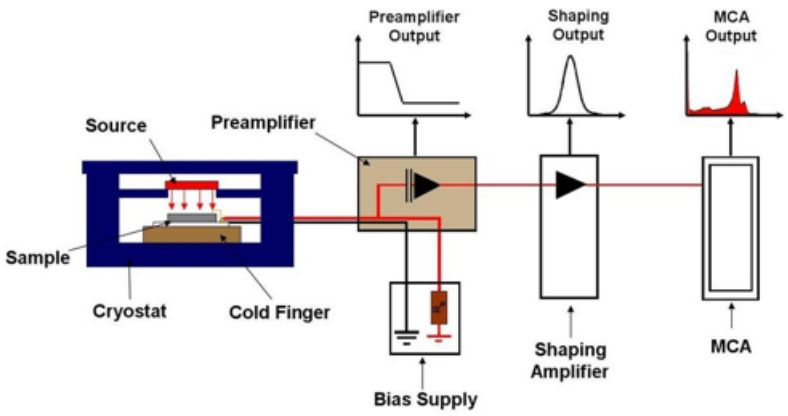

Figure 3.17: A schematic diagram of an alpha spectrometer (taken from [43])

A thin silicon detector and a thin sample are placed in a small vacuum chamber to eliminate energy loss in air for alpha particles. The insensitivity of alpha and beta semiconductor detectors to gamma radiation makes shielding unnecessary in most work. The chamber system is a shield for ambient background for alpha particles, other ambient radiation is not detected in the thin solid to any significant extent.

Alpha particles are emitted from nuclei with discrete energies which are characteristic of the source. Alpha emitting radionuclide may emit alpha particles of a single discrete energy or of several different energies, depending upon its nuclear properties. In either case, the energies of the alpha particles are well defined and may be used to characterize the emitting nuclide. Both qualitative and quantitative analyses may be made by measurements of the alpha energy spectra of suitable sources [80].

Chapter 4

Results, Analysis and Discussions

The aim of this study was to assess the levels of activity concentration of uranium isotopes in water samples taken near former uranium mines in the West Rand area of Johannesburg. The presence of ^{208}Pb, ^{209}Bi, ^{232}Th was also investigated. A batch of eleven water samples was collected from different locations within 30 km around the mines as discussed in Sect. 3.1. Water samples were separated three in groups, one was collected downstream of the mining operation and the other was collected upstream and lastly from tap water treatment facility from nearby mining community. As with all the analytical measurements, proper calibration relies on experimental technique to obtain quantitative results. In this work energy and efficiency calibrations of the detectors were done by counting a certified reference source (details of the source are in Sect. 3.3.2). Uranium isotopes were analyzed using the analytical procedures discussed in Chapter 3.4. The annual ingestion dose was calculated using the radioactivity concentrations for the uranium isotopes, as will be discussed in Sect. 4.4, which also shows the dose levels for the adult and infant groups (1 and 5 years). The dose conversion factors recommended by the International Commission on Radiation Protection and Measurement (ICRP) (1996) were utilized.

4.1 Overview of uranium isotopes activity

The radioactivity measurements were performed by means of Alpha Spectrometry as outlined in Sect. 3.4, see Fig. 3.11, in a low level background configuration at the National Nuclear Regulator Environmental Laboratory.

The method employed was based separation of uranium isotopes by Eichrom UTEVA resins prior to counting by alpha spectrometry as discussed in Sect. 3.2. The results of the measured samples is presented in Table 4.1 below. The activity value (X), the probable error on this value (s), and the minimum detectable activity (MDA) are all reported normally by NNR Laboratory. Only the activity concentration and uncertainty values are presented in Tables 4.1. The MDA values are excluded for easier understanding and presentation of the table. The primary sources of uncertainty include counting statistics in ^{234}U, ^{238}U and tracer peaks, systematic effects from choosing fixed regions of interest, tracer activity and mass, and sample volume. Another source of uncertainty in the chemical yield is that the uranium in the mineral water may behave differently from the tracer due to matrix effects [81].

The experimentally obtained uranium isotopes activity concentration values reported in mBq/l ranged from less than Minimum Detectable Activity (MDA) to 1300 ± 22.4 for June 2019, 3.0 ± 0.51 to 1091 ± 21.93 for September 2019, 1.0 ± 0.51 to 1294 ±24.2 for December 2019 and 1.0 ±0.06 to 984 ± 22.53 for March 2020. The measurement results of the sampling campaign in June 2019, winter seasons are all higher than the rest of the seasons. The highest observed was for Blyvoor collected downstream of the mining operation and Ezulwini outlet collected from Peter Wright dam. However, the activity concentration for all the other samples collected at Blyvooruitzich were observed to be higher than all the sampling points and were ranging from 521 mBq/l to 1300 mBq/l for ^{234}U and 491 mBq/l to 1193 mB/l for ^{238}U. The activity concentration could be high due to the fact that its a downstream discharge point.

The highest observed activity concentration for ^{235}U is 60 mBq/l. Ezulwini sampling point is the second sample point with the highest activity concentration as shown in Table 4.1. The lowest activity concentrations were detected in drinking water at the Driefontein sampling point in June 2019, this was expected as it was used as a control sample. September 2019 had the highest activity of 102±7.35 mBq/l. The uranium isotopes activities of water samples collected from the former mining sites across West-Rand area of Johannesburg are graphically presented in Figs. 4.1 to 4.4 for all the four seasons. The percentage contribution of total uranium isotopes activity concentration in each sample region during the surveyed seasons is shown in Fig. 4.5 .With the exception of autumn samples, the uranium isotopes activity concentrations reported in all four investigated seasons were nearly uniformly distributed. The

autumn season, which is the sampling campaign that begins in March 2020, has the lowest concentration of total uranium isotopes activity concentration as shown in Fig. 4.5 with about 22.2 % of the total contribution of uranium isotopes as compared to the highest of 27.5 % for winter samples. The percentage contribution for September and December sampling campaign were evenly distributed as they were close to one another.
The uranium isotopes activity in the drinking water sample is minimal as expected. This could attributed to the fact that the water has been treated for domestic use. The range for ^{234}U, ^{235}U and ^{238}U is < MDA to 102±7.35 mBq/l, < MDA to 3±1.45 mBq/l and 5±1.85 mBq/l to 70±6.25 mBq/l respectively. The Department of Water and Sanitation, DWS [formerly known as the Department of Water Affairs], provides radiological recommendations in Ref. [82]. For radioactivity, a Target Water Quality Range (TWQR) or "no-effect range" for ^{238}U was provided to be 0.890 Bq/l and was used to evaluate the quality of water. The measured average of 1.05 Bq/l for ^{234}U exceeded the TWQR value of 0.890 Bq/l for all the sample collected at Blyvooruitzich (Bly4) for all the seasons. For ^{238}U, the measured average value of 0.957 exceeded the TWQR value for all sample collected at Blyvooruitzich (Bly4) for all the seasons, with the exception of samples taken in March 2020. ^{238}U levels exceeded the TQWR for all the samples collected at Blyvooruitzich combination and Peter Wright –outlet. The average TQWR values for both the sampling points were found to be 1.07 and 1.05. Samples collected at Peter Wright –intlet in December also exceeded the TQWR. Renal toxicity can occur in sensitive people with impaired renal function, but renal toxicity in healthy people is uncommon. TQWR was not exceeded for the other sampling point. The WHO guideline values of 10 Bq/l, 1 Bq/l and 10 Bq/l for ^{234}U, ^{235}U and ^{238}U, respectively, was not exceeded in the drinking water samples, including all the other samples. Because the samples were filtered before being measured as described in section 3.2.2, the radioactivity in the samples were effectively reduced. For example, uranium isotope concentrations were low in the filtered water samples, since some of the uranium was present in the particulate matter and therefore removed by filtration.

The water's physical and aesthetic properties were also determined. The measured Electrical conductivity (EC) varied between 1930 and 11700 mS/m [83]. The EC values were higher than the South African water quality guideline of 1200 mg/l [3]. A correlation between (EC) and radioactivity was observed - in most cases the samples with high EC were also associated with high uranium

concentrations. The average EC obtained were from 3134, 5566, 2872 and 3086 mS/m for collected samples in June 2019, September 2019, December 2019 and March 2020, respectively. Uranium isotopes were detected in all the samples and hence the EC exceeded the SANS:241:1 guideline limit.

Table 4.1: ^{234}U, ^{235}U, and ^{238}U activity concentrations in water samples from the study area.

Sample ID	**Jun-19**			**Sep-19**			**Dec-19**			**Mar-20**		
	234 U (mBq/l)	**235 U (mBq/l)**	**238 U (mBq/l)**	**234 U (mBq/l)**	**235 U (mBq/l)**	**238 U (mBq/l)**	**234 U (mBq/l)**	**235 U (mBq/l)**	**238 U (mBq/l)**	**234 U (mBq/l)**	**235 U (mBq/l)**	**238 U (mBq/l)**
A1	1300 ±25	53± 4.99	1193 ±24	1046±21.3	48±5.51	860±19.43	958±22.23	60±5.55	818±20.61	883±19.96	31±3.71	778±18.75
A2	529 ± 15	23.0 ±3.18	491±14.7	682±18.01	23±3.22	569±16.49	582±16.17	23±3.17	511±15.18	563±20.22	45±5.67	507±19.17
A3	1261±24	49 ±4.8	1176±23	953±20.77	34±3.87	783±18.87	1294±24.2	41±4.27	817±19.21	620±16.81	21±3.05	546±15.74
A4	424±13.86	16±2.67	398±13.35	427±13.96	15±2.62	367±12.99	328±12.31	8±1.87	264±11.08	142±8	5.64±0.32	122±7
A5	579±16.85	23±3.4	458±15	631±16.6	19±2.95	494±14.72	603±16.64	18±2.82	529±15.66	178±8	9.09±0.39	197±8
A6	510±15.24	21±3.11	433±14.1	677±17.46	17±2.68	5.27±15.43	570±15.95	23±3.22	4.91±14.82	482±14	26.8±0.7	583±15
A7	146±8.48	6±1.8	160±9.0	267±10.64	13±2.23	2.32±9.96	207±9.61	9±2.01	185±9.1	331±12	14.8±0.5	321±11
A8	322±17.96	9±3.13	315±18.14	316±15.9	19±3.74	222±13.29	108±9.73	5±1.97	78±8.73	473±15	22.2±0.7	482±15
A9	1007±22.25	44±4.41	1086±22.10	1091±21.93	48±4.55	1087±21.96	1102±22.03	48±4.57	1126±22.29	984±22.53	33±4.18	974±22.41
A10	803±19.43	38±4.22	827±19.67	796±18.46	38±3.99	817±18.79	1071±22.82	44±4.6	1035±22.36	807±20.18	37±4.35	815±20.3
A11	<MDA	<MDA	5±1.85	102±7.35	3±1.45	70±6.25	5±1.30	1±0.51	3±0.84	7±1.89	1±0.6	4±1.18

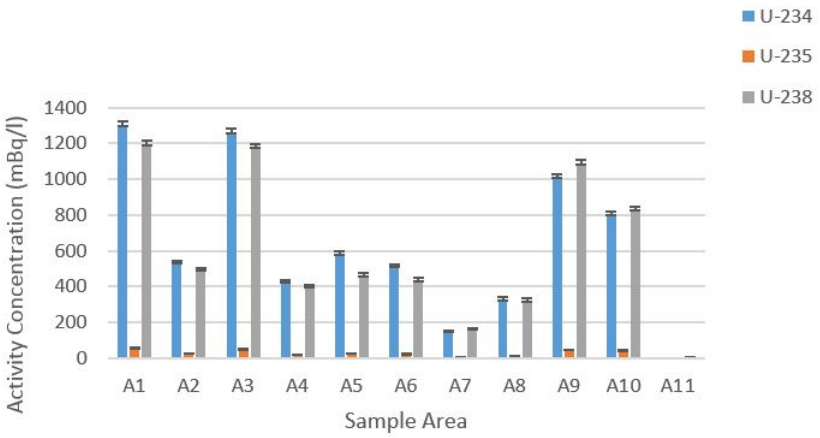

Figure 4.1: June 2019 Activity concentration results for uranium isotopes considered

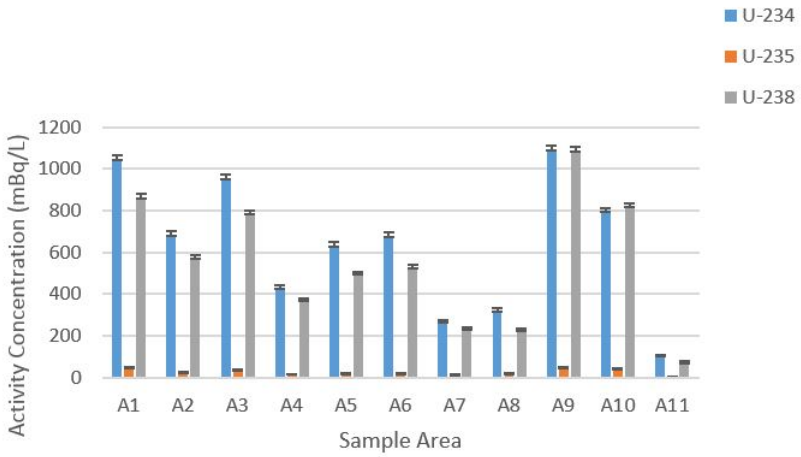

Figure 4.2: September 2019 Activity concentration results for uranium isotopes considered

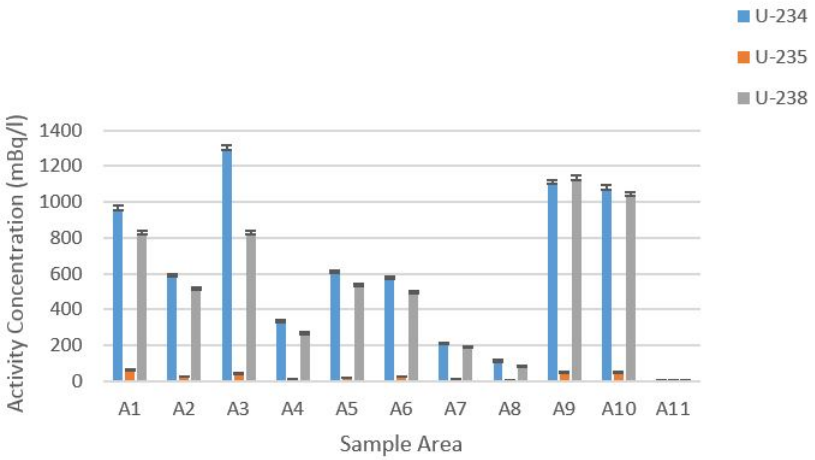

Figure 4.3: December 2019 Activity concentration results for uranium isotopes considered

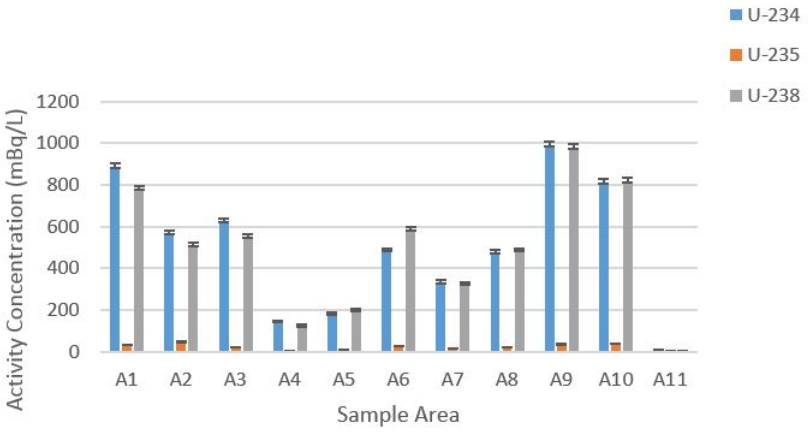

Figure 4.4: March 2020 Activity concentration results for uranium isotopes considered

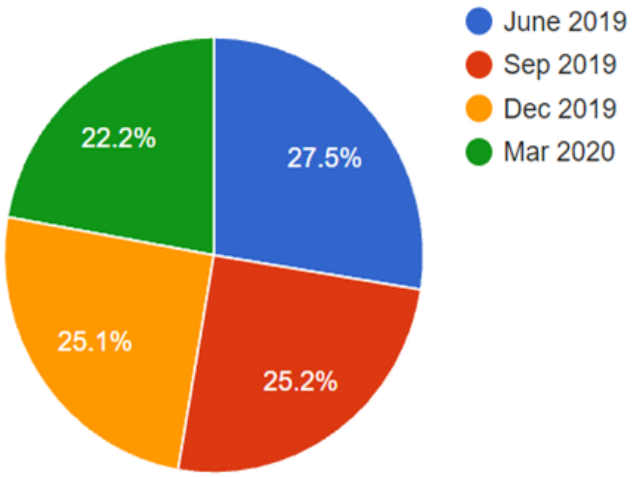

Figure 4.5: Percentage contribution to the total uranium isotopes activity concentrations in water samples in the four surveyed seasons in the current study.

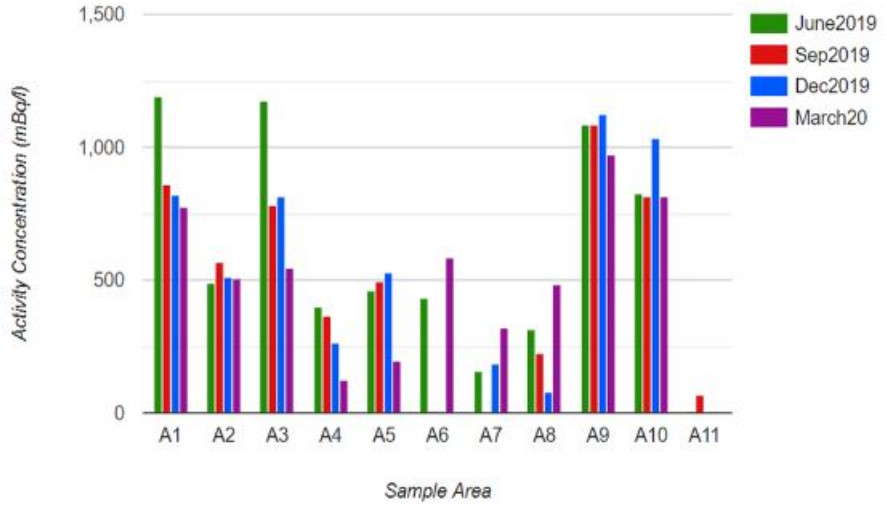

Figure 4.6: Uranium 234 Activity concentration results for all seasons at different sampling areas

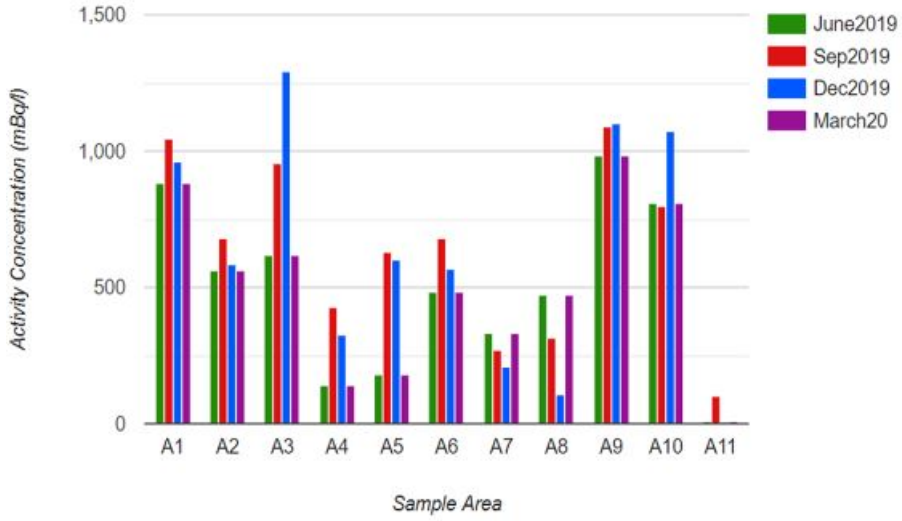

Figure 4.7: Uranium 238 Activity concentration results for all seasons at different sampling areas

The quality of water from the mining and NORM industries varied, with somewhat high activity detected in some surface water samples from gold mine areas, indicating a potential radiological health risk from ingestion of this water, which was definitely impacted by process water. The $^{234}U/^{238}U$ ratio may be influenced by the total uranium activity contained in water. The isotopic ratios of $^{234}U/^{238}U$ was determined to be between 0.82 to 1.58 for all the water samples during the current sampling period. This is a clear indication that mining activities had a significant impact on the water sources in all sampling area. In these water samples with apparent disequilibrium, measuring just ^{238}U would have resulted in an underestimating of overall uranium activity. And hence all the uranium isotopes were determined.

According to Ref. [84], around 80 % of samples with a high ratio of disequilibrium (> 1.6) had the lowest uranium activity concentration (less than 100 mBq/l). In this case, the uranium isotopic ratio for drinking water collected at driefontein was between 1.66 to 1.75. Samples having a low ratio (< 1.5) correlate to uranium activity concentrations greater than 200 mBq/l. Activity concentrations of ^{234}U were observed to be higher than activity concentrations of ^{238}U as shown in Figure 4.6 and 4.87. This indicates that there is no radioactive equilibrium between uranium 234 and uranium 238 in the collected samples. The isotopic ratio can be used to determine the source of uranium in water, with a ratio near unity indicating that the water may have been

contaminated by uranium-bearing ores. Isotopic analysis is critical for accurately estimating uranium dose due to the disequilibrium between ^{234}U and ^{238}U that may be found in water. The dose can be underestimated if just ^{238}U is measured (by chemical approach) and equilibrium is assumed. The mass of uranium is mostly dictated by ^{238}U due to its longer half-life and percentage of abundance, although the activity of all three uranium isotopes will contribute to the total activity concentration in the water. As a result, the activity concentrations of each of the three uranium isotopes must be determined in order to convert mass to activity or vice versa accurately.

4.2 Pb, Bi and Th elemental composition in the measured samples

Elemental concentrations of ^{208}Pb, ^{209}Bi and ^{232}Th were determined by ICP-MS analytical technique as described in section 3.3.3. Table 4.2 estimates the detection limits of Pb, Bi, and Th between 0.124 and 2.86 ppb. Samples were collected in June 2019 at different sampling points in the former uranium mines as shown in Table 4.2. Measured ^{208}Pb elemental concentration values ranged from 5.99 to 6.63 ppb. As shown in Table 4.2, the percentage Relative Standard Deviation (RSD) values are in the same order of magnitude, ranging from 1.0 to 3.6. Standard limit of 10ppm was not exceeded for Lead as indicated [3]. ^{209}Bi elemental concentrations in water samples ranged from 0.81 to 1.27 ppb, as shown in Table 4.2, the RSD values ranged from 6.60 to 26.40. However, since the instrumental intensity for ^{209}Bi is approaching the lower limit of detection, RSD may be limited by counting statistics. Finally, the measured concentration of ^{232}Th, in the collected samples, was in the range of 2.63 to 7.21 ppb. The average thorium value was 4.39 ppb, with the RSD ranging from 1.10 to 15.20. The guidance level of 1.0 Bq/l was not exceeded, the highest calculated activity concentration of thorium-232 was 0.03 Bq/l (7.21 ppb). The calculated thorium value was lower than the reference value of 0.05 mBq/l for ^{228}Th and ^{232}Th [46].

Table 4.2: Isotopic concentrations of ^{208}Pb, ^{209}Bi and ^{232}Th in the measured samples.

ICP-MS Isotopic concentration (ppb)							
Sample No.	Sample Area	Pb-208	RSD	Bi-209	RSD	Th-232	RSD
A1	Blyvooruitzich (Bly4)	6.63	1.00	0.84	11.60	5.56	5.70
A2	Blyvooruitzich (Bly6)	6.15	1.70	0.96	16.50	4.71	1.10
A3	Bly comb	5.99	4.00	0.82	17.40	4.19	4.70
A4	Driefontein	6.56	2.00	1.27	26.40	7.21	2.60
A5	Ezulwini	6.71	2.00	0.85	6.60	3.45	15.20
A6	Ezulwini-in	6.36	3.60	0.82	18.80	2.63	12.10
A7	Drinking water	6.68	3.20	0.81	21.60	3.03	3.80

4.3 Uranium Isotopes Dose Assessment

Water consumption, being a necessary component of the human diet, may contribute to natural radioactivity exposure, albeit this contribution is normally minor and may be regulated and limited by safety standards. Because human industrial activities may enhance the radiation contribution from water, radiometric analyses of water and dose calculations are significant in environmental assessment. Radioactive discharges from mining and mineral operations, which can have an impact on water quality, should be controlled and monitored to ensure the population consuming this water is exposed to the permissible dose levels. The risk of intake must be assessed against the dose limit of 1 mSv/a or dose constraint of 0.25 mSv/a as stipulated in the NNR Act Number 47 of 1999 [85].

Regulations on radioactivity levels in drinking water have been issued by the World Health Organization (WHO), the United States Environmental Protection Agency (US EPA) [50], and the European Union (EU). Many countries like South Africa have followed WHO recommendations and launched radiation monitoring programs to ensure that drinking water is safe to drink. EU member states are obliged to adhere to the requirements outlined in the 2013 directive [86]. The South African Department of Water and Sanitation regulates water quality in the country. Since 2006, a National Monitoring Program for Radioactivity (NMPR) has been in place to assess the radiological quality of these water sources and their effect on the public who consume them as part of their daily diet [7]. There were no legal legislation in existence in South Africa at the time of this study requiring the monitoring of radioactivity

in drinking water, but South African organizations, such as SANS 241, had set limits based on WHO recommendations. The radioactivity of some of the sources of drinking water in South Africa is not routinely monitored, with the exception of the NMPR survey, which is limited to select catchments.

4.3.1 Annual dose criteria

Dose rates were calculated according to the NNR RG-002 [1], water consumption rate for different age groups and dose conversion factors published in IAEA Safety Standards General Safety Requirements Part 3 [87] were used. Dose was modeled for various age groups to ascertain the contribution of uranium isotopes to the total dose of a person consuming the water on a regular basis. The criterion also includes consideration of detected radioactivity levels in the water samples, where ingestion pathway is not practical in order to determine if there is radiological contamination in the environment. The measured individual radioactivity concentrations were used to calculate the annual ingestion dose using the lifetime age-weighted approach as expressed in Eq. (4.1), including the corresponding dose conversion factors for all age groups in Table 4.3, also showing the dose values for the adult and infant groups. Based on regulatory guidelines in Ref. [1], water consumption was calculated based on annual intake (see Table 4.2,). The sum of all doses with proportional contributions for the various age groups corresponds to the lifetime average annual dosage:

$$D_i(x) = \Sigma_p A_i p C_p(x) DCF_i(x) \tag{4.1}$$

where, $D_i(x)$ is the annual dose to an individual from age group x (Sv/a)
$A_i(p)$ is the activity concentration of nuclide i in product p (Bq/l)
$C_p(x)$ consumption rate of product p for individuals of age group x *(l/a)*
$DCF_i(x)$ is the dose coefficient for ingestion of nuclide i and age group x *(Sv/Bq)*

Table 4.3: Dose conversion factors (Sv/Bq) used to calculate human ingestion dose and Annual Consumption – humans L/a.

Conversion Factors (Sv/Bq)					
Nuclide	**1 year old**	**5 year old**	**10 year old**	**15 year old**	**Adult**
U-234	1,30E-07	8,80E-08	7,40E-08	7,40E-08	4,90E-08
U-235	1,30E-07	8,50E-08	7,10E-08	7,00E-08	4,70E-08
U-238	1,20E-07	8,00E-08	6,80E-08	6,70E-08	4,50E-08
Annual Consumption Factors					
Volume	**1 year old**	**5 year old**	**10 year old**	**15 year old**	**Adult**
l/a	240	300	360	510	600

4.3.2 Dose Evaluation

Annual dose calculations are presented graphically in Figs. 4.8 - 4.11 for both the adult and infant age groups. Eq. (4.1) was used to calculate the dose. The dose limit of 1.0 mSv/a was not exceeded in any of the samples for all the age groups. The National Nuclear Regulator dose constraint of 0.25 mSv/a was also not exceeded for all age groups in all the samples. As shown in Figs. 4.8-4.11 the calculated doses in water ranged between 0.00014 and 0.092 mSv/a. In the 15 years and 1 year age groups, the highest calculated doses were observed for all the seasons. This could be due to high dose conversion factors for the infant groups, and the conservative assumption that infants consume 200 litre of water per annum. This would result in a potential exposure if this water had been for drinking purposes, which was not expected to be the case. There was a slight decrease in calculated doses for all the other samples collected in September 2019, December 2019 and March 2020 compared with the doses calculated for the June 2019 samples as shown in Table 4.7. There is a good correlation of the calculated standard deviation for the doses of different age groups as shown in table 4.4. The highest values were observed for the 15 years age group ranging from 0.022 to 0.031, and the lowest values were observed for the 5 years age group.

The evaluation of the drinking for the water quality was based on results obtained over a period of four seasons. When looking at the contribution of all the uranium isotopes to the dose, ^{234}U contribution was higher in all the samples as compared to ^{238}U as shown in Figs. 4.8 to 4.11, this could be due to

very high dose conversion factors of ^{234}U. ^{235}U dose contribution was confirmed as the lowest found in the measured activity concentration.
As shown in Figs. 4.8 - 4.11, the guidance levels for the radionuclide concentration provided in the WHO Guidelines for drinking water quality, was not exceeded in the collected water samples. This guidance level is based on individual dose criterion of 0.1 mSv committed effective dose. It is evident from the graph presented in Fig. 4.8 that samples collected at Blyvoor had dose rates close to the WHO guidance level for 1 year and 15 year age groups. The doses were 0.08 mSv/a and 0.09 mS/a for the age group mentioned above, this is due to high measured activity concentrations dose conversion factors and consumption rates. The annual ingestion dose for ^{238}U in the samples collected in the current study were higher than the European Commission, lower that the World Health Organization and National Nuclear Regulator dose constraint. The results of this study indicate that the total annual effective doses from the intake of ^{234}U, ^{235}U and ^{238}U radionuclides in water samples collected in the West-Rand area were below the World Health Organisation (WHO) guidance limit of 0.1 mSv/a as well as the NNR dose constraint of 0.25 mSv/a. The dose results could be an indication that these sampling areas were treated before being discharged into the environment. In most cases, the amount and quality of mine effluent discharged into the environment are regulated. Depending on the water quality improvement, settling ponds are used to improve the quality of water before it is released.

Table 4.6 shows the radioactivity classes, according to [16], in which the annual average radioactivity dose for the sample sites are categorised. The collected sampling points are classified from the radiological point of view for drinking water in the ideal class (dose 0 to 0,1 mSv/a); All the sampling areas were found to be in class 0. There were no sampling areas in the yellow class or higher class (<1 mSv/a). This implies that there is no indication that intervention is required. Only 2 sampling areas showed marginal radioactivity status for the 1 year old age group, who are the most sensitive class for radioactivity status of water. The two latter sampling areas were Blyvooruitzich (Bly4) and Blyvooruitzich combination.

Table 4.4: Calculated standard deviation for the annual doses for the study area.

Season	1 year old	5 year old	10 yrs old	15 yrs old	Adult
Jun-19	0.026	0.022	0.022	0.031	0.024
Sep-19	0.019	0.016	0.017	0.022	0.018
Dec-19	0.025	0.021	0.021	0.030	0.023
Mar-20	0.019	0.016	0.016	0.023	0.018

4.3.3 Excess lifetime cancer risk

Estimation of the Excess Lifetime Cancer Risk (ELCR) is also taken into account in this research. By calculating the additional lifetime cancer risk associated with the average intake of uranium isotopes in water samples, the probability of developing cancer throughout a lifetime can be predicted. This is considered as probable carcinogenic effects based on exposures and dose-response data that estimate the chance of cancer incidence in a population of persons over a certain lifetime. The ELCR was calculated for the age group with the highest dose which was for 15 years age group. All the other age groups will not have the ELCR higher that this group. Equation (2.40) was used to calculate the ELCR values as shown in the Table 4.5. The risk due to the consumption of water was calculated to be in the range 6.78E-04 to 3.66E-01 for samples collected at Blyvooruitzich (Bly4) and drinking water from Driefontein, the highest risk found in samples collected in June 2019 as shown in Fig. 4.8, (0.09 mSv/a and 1.7E-04 in June 2019). The calculated standard deviation for ELCR was 0.123, 0.094, 0.119 and 0.090 for June 2019, September 2019, December 2019 and March 2020 respectively. The values are of the same order of magnitude. The average of 1.0E-04 as per the WHO for drinking water was exceeded. The elevated levels of uranium and its associated risk in the water samples could be attributed to mineralisation. Although the dose constraint for drinking water was not exceeded, sample specific investigation need to be carried out to determine the ELCR for drinking water.

Table 4.5: Excess Lifetime Cancer Risk (ELCR) for ingestion of uranium isotopes for 15 years age group.

Sample No.	**June 2019**	**Sept 2019**	**Dec 2019**	**Mar 2020**
A1	3.66E-01	2.82E-01	2.62E-01	2.43E-01
A2	1.50E-01	1.84E-01	1.52E-01	1.60E-01
A3	3.57E-01	2.55E-01	3.12E-01	1.71E-01
A4	1.20E-01	1.16E-01	8.65E-02	3.88E-02
A5	1.53E-01	1.65E-01	1.66E-01	5.49E-02
A6	1.39E-01	1.76E-01	1.56E-01	1.56E-01
A7	4.46E-02	7.37E-02	5.77E-02	9.57E-02
A8	9.27E-02	8.06E-02	2.76E-02	1.40E-01
A9	3.06E-01	3.19E-01	3.26E-01	2.86E-01
A10	2.39E-01	2.37E-01	3.09E-01	2.38E-01
A11	6.78E-04	2.53E-02	1.32E-03	1.76E-03

Table 4.6: Radiation dose classification for drinking water with health effects and intervention time frames indicators. [88]

Dose class	**Color**	**Dose range (mSv/a)**	**Health Effects**	**Intervention indicators time frame**
Class 0, (ideal quality)		0.01–0.1	No observable health effects	No intervention required
Class 1, (good quality)		>0.1–1	No observable health effects	No intervention required, but ALARA principle applies
Class 2, (marginal quality)		>1–10	Small increase in cancer mortality risk	Consider intervention within 2 years
Class 3, (poor quality)		>10–100	Cancer risk statistically detectable in very large population groups	Intervention required within 1 year
Class 4, (unacceptable quality)		>100	Health effects clinically detectable	Immediate intervention required.

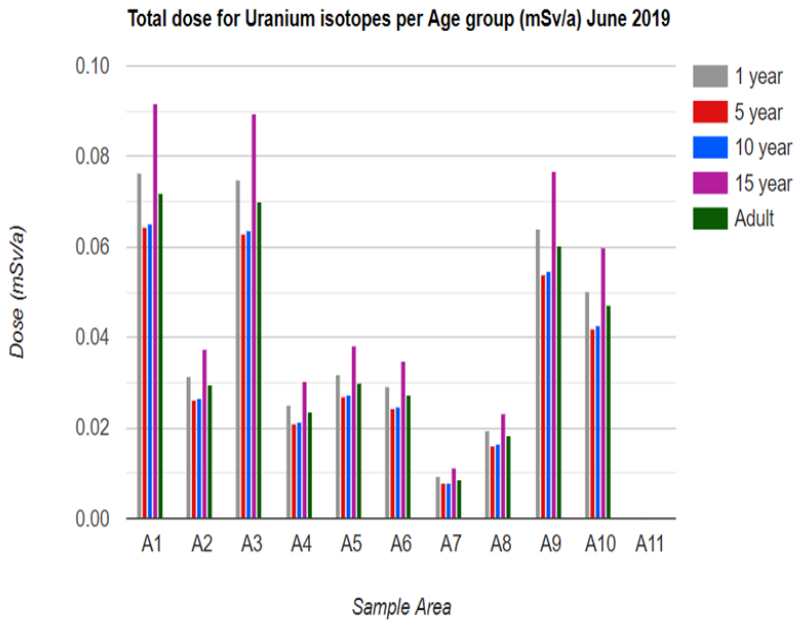

Figure 4.8: Estimated total doses from uranium isotopes for different age groups for June 2019

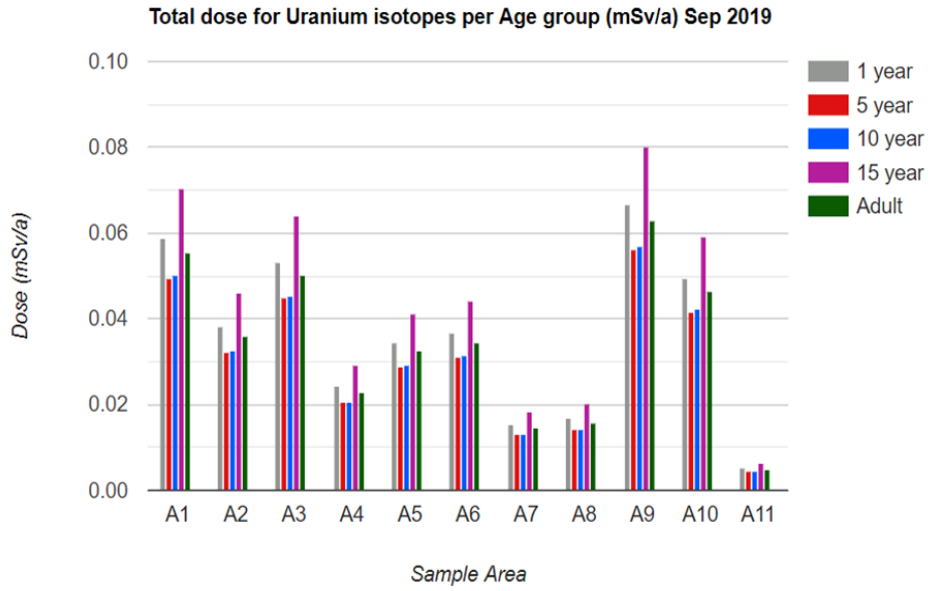

Figure 4.9: Estimated total doses from uranium isotopes for different age groups for September 2019 results

Table 4.7: Annual dose (mSv/a) calculated for June 2019 and September 2019 water samples.

Sample No	1 year old	5 year old	10 yrs old	15 yrs old	Adult	1 year old	5 year old	10 yrs old	15 yrs old	Adult
	Jun-19					Sep-19				
1	0,07654	0,06428	0,06517	0,09168	0,0719	0,0589	0,04948	0,05015	0,07058	0,05533
2	0,03136	0,02634	0,0267	0,03756	0,02946	0,03838	0,03225	0,03269	0,046	0,03606
3	0,07474	0,06276	0,06363	0,08952	0,07021	0,05334	0,04483	0,04542	0,06394	0,05012
4	0,02519	0,02115	0,02145	0,03017	0,02366	0,02436	0,02046	0,02074	0,02919	0,02289
5	0,03197	0,02686	0,02722	0,03832	0,03004	0,03451	0,029	0,02939	0,04137	0,03243
6	0,02904	0,02439	0,02472	0,03479	0,02728	0,03683	0,03095	0,03137	0,04416	0,03461
7	0,00935	0,00785	0,00796	0,01119	0,00878	0,01542	0,01295	0,01312	0,01847	0,01448
8	0,0194	0,01629	0,01652	0,02324	0,01823	0,01685	0,01415	0,01434	0,02019	0,01582
9	0,06407	0,05377	0,05454	0,07668	0,06017	0,06684	0,05611	0,0569	0,08003	0,06278
10	0,05006	0,04202	0,04261	0,05992	0,04701	0,04955	0,04159	0,04218	0,05931	0,04653
11	0,00014	0,00012	0,00012	0,00017	0,00014	0,00529	0,00445	0,00451	0,00635	0,00497

Table 4.8: Annual dose (mSv/a) calculated for December 2019 and March 2019 water samples.

Sample No	1 year old	5 year old	10 yrs old	15 yrs old	Adult	1 year old	5 year old	10 yrs old	15 yrs old	Adult
	Dec-21					Mar-20				
1	0,05498	0,04612	0,04678	0,06575	0,05161	0,0589	0,04948	0,05015	0,07058	0,05533
2	0,03191	0,02679	0,02716	0,03821	0,02997	0,03838	0,03225	0,03269	0,046	0,03606
3	0,06518	0,05482	0,05552	0,07822	0,06126	0,05334	0,04483	0,04542	0,06394	0,05012
4	0,01809	0,0152	0,01541	0,02169	0,017	0,02436	0,02046	0,02074	0,02919	0,02289
5	0,03461	0,02907	0,02947	0,04148	0,03252	0,03451	0,029	0,02939	0,04137	0,03243
6	0,03264	0,02742	0,02779	0,03911	0,03066	0,03683	0,03095	0,03137	0,04416	0,03461
7	0,01207	0,01013	0,01027	0,01445	0,01133	0,01542	0,01295	0,01312	0,01847	0,01448
8	0,00577	0,00485	0,00491	0,00692	0,00542	0,01685	0,01415	0,01434	0,02019	0,01582
9	0,06831	0,05734	0,05815	0,08178	0,06415	0,06684	0,05611	0,0569	0,08003	0,06278
10	0,0646	0,05424	0,05499	0,07736	0,06067	0,04955	0,04159	0,04218	0,05931	0,04653
11	0,00027	0,00023	0,00023	0,00033	0,00026	0,00529	0,00445	0,00451	0,00635	0,00497

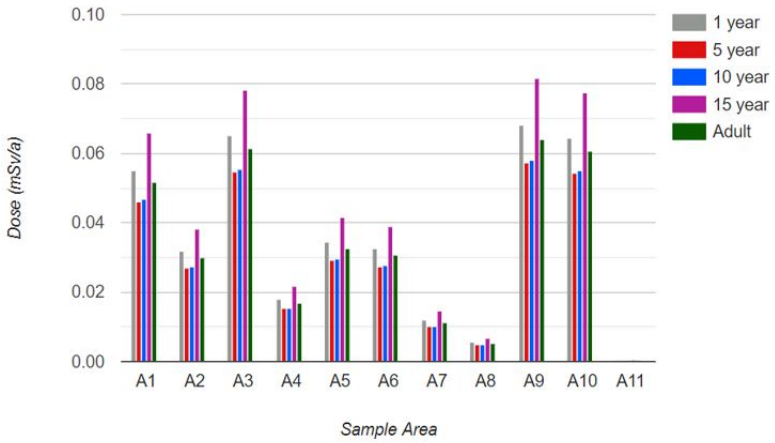

Figure 4.10: Estimated Total dose for uranium isotopes for different age groups for December 2019 results

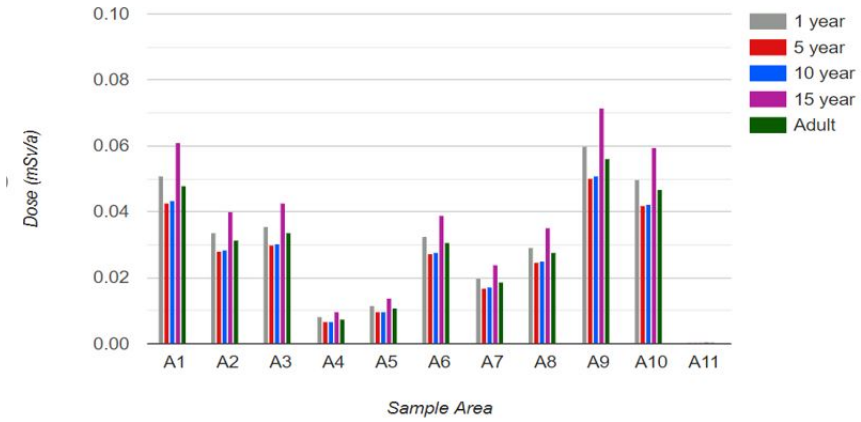

Figure 4.11: Estimated Total dose for uranium isotopes for different age groups for March 2020 results

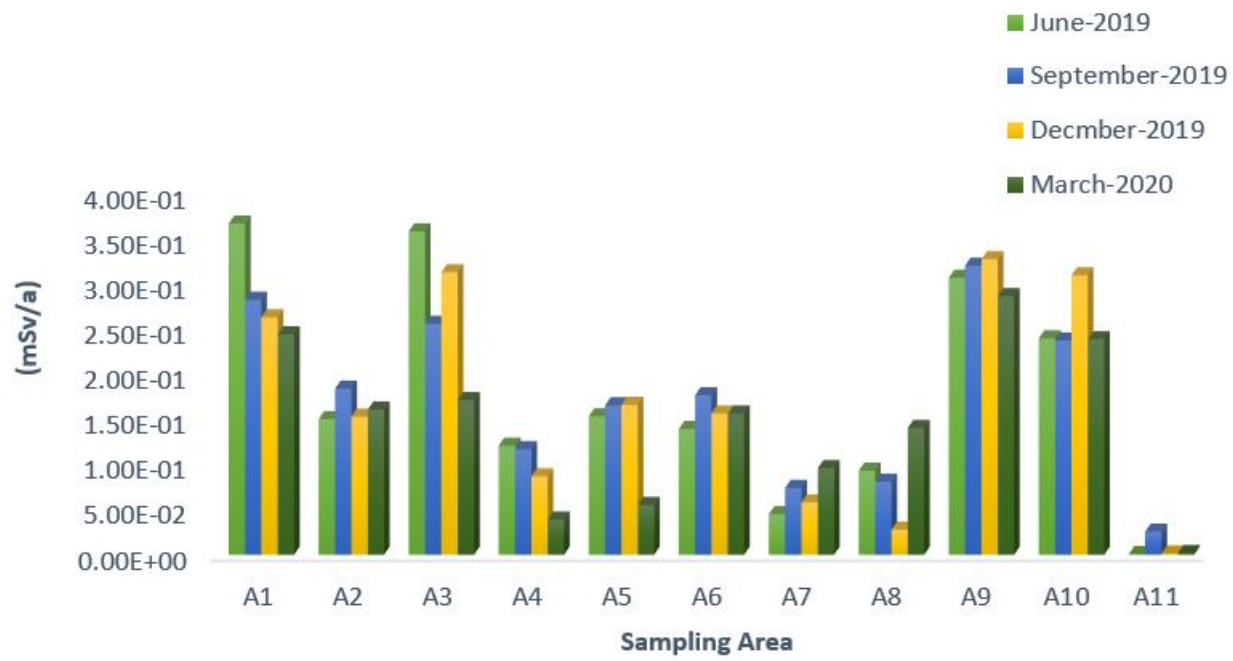

Figure 4.12: Bar graph showing ELCR fo uranium isotopes in water samples at different mining locations in West-Rand area

4.4 Statistical analysis of results

A student T-test can be used to determine the difference in the means of two mutually independent groups. The one-way ANOVA, on the other hand, is the most used method for determining the differences in means of three or more groups. The F-test is another name for the ANOVA test [83]. The data on uranium isotopes was subjected to an analysis of variance (ANOVA) to see if the differences in the results of the samples under examination were statistically significant. Tables A1 to A3 show the F-value, significant P-value, and F-critical values for the samples.

The mean activity (mBq/l) values are shown in Tables A1 to A3 for ^{234}U, ^{238}U, and ^{235}U for the samples collected from June 2019 to March 2020, as demonstrated by the one-way Anova. The observed mean value for ^{234}U as shown in Table A1 to A3 showed the mean value is significantly different <p 0.05. ^{238}U and ^{235}U showed that mean values of 0.0001 and 0.00009, respectively are significantly different with p less than 0.05, as tabulated in Table A2. The F-value for December 2019 was the lowest as compared to sample

campaign in June, September and March 2020, which indicates a very low probability that the differences were just a coincidence. Appendix A Tables A4 to A7 show that the mean annual effective dose of Uranium isotopes extracted from samples analysed during consecutive June 2019 and March 2020 seasons is not significantly different with p greater that 0.05. All confidence interval mean comparisons within a pair of groups show no statistically significant mean differences. The observed mean values for the calculated doses as listed in Tables A4 to A7 showed that the mean values are not significantly different. The mean values of the annual effective dose ranged from 0.5044 to 0.743 as tabulated in Tables A4 to A7.

Chapter 5

Conclusion

The primary goal of this research was to measure the levels of radioactivity of Uranium isotopes in water samples taken from various sampling locations near former Uranium mines in Johannesburg, Gauteng Province, South Africa. A total of 44 water samples were collected, and analysed applying Alpha spectroscopy using the radio-chemical methods described in Section 3.2.4 in order to determine the activity concentrations of ^{234}U, ^{235}U and ^{238}U. For each age group, the water quality was assessed based on annaul effective dose estimation. As discussed in Section 2.3.5, the methodology used dose coefficients to estimate dose from internal exposure. Where applicable, the results were additionally assessed using DWS categorization or WHO and EU standards. The following conclusions have been reached:

- The detected uranium isotopes were observed to be high for the samples collected in Blyvoor which is were the sample collected downstream of the mine. The observed activity concentration was ranging from 529 mBq/l to 1300 mBq/l.
- The Target Water Quality for ^{238}U ranged from 1.3 Bq/l to 0.142 B/l for the samples collected in the mining area. Blyvooruitzich (Bly4) and Blyvooruitzich combination exceeded the TWQ of 0.89 B/l recommended by DWS, whereas the other samples did not exceed the TWQ.
- The differences in uranium isotopes activity concentrations in water samples could be related to differences in geological formation, geographical location of these places, and the length of time each mining area was open for business.
- The isotopic activity ratio of ^{234}U/^{238}U for the samples under study was

ranging from 1.66 to 1.75 %. The ratios confirms that the samples are from mining activities as per UNSCEAR and the activity concentrations of most of the samples were above 200m Bq/l.

- Total Dissolved Solids (TDS) and radioactivity were shown to be related in most situations, with high TDS samples also having high uranium contents.

- The annual ingestion doses for uranium isotopes in the current study were lower than the European Commission and the World Health Organization. The results of this study indicate that the total annual effective doses from the intake of ^{234}U,^{235}U and ^{235}U radionuclides in water samples collected in the West-Rand area were below the World Health Organisation (WHO) guidance limit of 0.1 mSv/a as well as the NNR dose constraint of 0.25 mSv/a.

- The obtained measured results show that the selected water sources in the West-Rand area are safe for domestic use or drinking when purification and treatment has been applied.

- The probability of acquiring cancer over the course of a lifetime associated with the average ingestion of uranium isotopes in the examined water samples was assessed using the excess lifetime cancer risk (ELCR), which was found to be very low.

- After a year of data collection, the results showed that the 11 sampling areas covered by the study were in the ideal class, showing no radioactivity concern.

5.1 Recommendations

To manage the current and potential consequences at the Gold Mines, the following are recommended.

- Water quality monitoring is required by the National Water Act 1998 (Act 36 of 1998) throughout the operation lifetime of any mine, whether or not there are discharges from mining operations. The water quality monitoring will guarantee that any possible sources of pollution are identified and addressed before they cause significant environmental harm.

- As part of its compliance assurance program, the National Nuclear Regulator (NNR) maintains an independent verification program. The NNR is mandated to produce and submit an annual report on health and safety issues for workers, the public, and the environment under Section 7(j) of the NNR Act (Act No. 47 of 1999). To achieve this criterion, independent verification of radiological environmental analysis is carried out, which entails collecting samples for radio-analysis near the mining facilities. The NNR should therefore, continue with the current surface water monitoring program as part of its regulatory requirements.

- literature suggests that the results between the ICP-MS and Alpha spectrometry should be comparative even though there might be challenges with the levels of detections. Therefore, similar research on water samples from the same sampling locations in the West-Rand should be investigated for the analyses of uranium, thorium and radium isotopes using Alpha Spectrometry (AS) and ICP-MS.

- The research should also include samples such as boreholes, sediments and vegetation in the same sampling area to assess transfer of nuclides from water to sediments and vegetation. The study should also evaluate the level of toxic heavy metals in and around the vicinity of the mine.

Bibliography

[1] National Nucler Regulator. *Safety assessment of radiation hazards to members of the public from NORM activities RG-002*. 2012.

[2] World Health Organization et al. Guidelines for drinking-water quality: second addendum. vol. 1, recommendations. 2008.

[3] SANS. South african national standard 241-1: Drinking water. part 1: Microbiological, physical, aesthetic and chemical determinands, 2015.

[4] Monty Charles. Unscear report 2000: sources and effects of ionizing radiation. *Journal of Radiological Protection*, 21(1):83, 2001.

[5] Frank Winde and EJ Stoch. Threats and opportunities for post-closure development in dolomitic gold mining areas of the west rand and far west rand (south africa)–a hydraulic view part 1: Mining legacy and future threats. *Water SA*, 36(1), 2010.

[6] Caspah Kamunda, Manny Mathuthu, and Morgan Madhuku. An assessment of radiological hazards from gold mine tailings in the province of gauteng in south africa. *International Journal of environmental research and public health*, 13(1):138, 2016.

[7] INSTITUTE FOR WATER QUALITY STUDIES. Report on the radioactivity monitoring programme in the mooi river (wonderfonteinspruit) catchment, 1999.

[8] Henk Coetzee, F Winde, and PW Wade. *An Assessment of Sources, Pathways, Mechanisms and Risks of Current and Potential Future Pollution of Water and Sediments in Gold-mining Areas of the Wonderfonteinspruit Catchment: Report to the Water Research Commission*. Water Research Comission, 2006.

[9] National Research Council et al. Uranium mining in virginia: scientific, technical, environmental, human health and safety, and regulatory aspects of uranium mining and processing in virginia. 2012.

[10] Samantha Richardson. *Sinkhole and subsidence record in the chuniespoort group dolomite, Gauteng, South Africa*. PhD thesis, University of Pretoria, 2013.

[11] J.F. Durand. The impact of gold mining on the witwatersrand on the rivers and karst system of gauteng and north west province, south africa. *Journal of African Earth Sciences*, 68:24–43, 2012.

[12] World Health Organization et al. Uranium in drinking-water: background document for development of who guidelines for drinking-water quality. Technical report, World Health Organization, 2004.

[13] Rati Varshney. *natural radioactivity and Radon/Thoron measurement in environment & quantification of heavy elements*. PhD thesis, Aligarh Muslim University, 2013.

[14] Change Laura Tan. Big gaps and short bridges: A model for solving the discontinuity problem. *Answers Research Journal*, 9:149–162, 2016.

[15] OK Hakam, A Choukri, Z Moutia, A Chouak, R Cherkaoui, J-L Reyss, and M Lferde. Uranium and radium in groundwater and surface water samples in morocco. *Radiation Physics and Chemistry*, 61(3-6):653–654, 2001.

[16] I Sekoko, A Kuhn, P Kempster, B Madikizela, H van Niekerk, M van Veelen, and J Slabbert. Design of a national radioactivity monitoring programme(nrmp) to monitor surface water resources in south africa. *Water Pollution VIII: Modelling, Monitoring and Management.*, 1:357–366, 2006.

[17] Godfred Darko, Augustine Faanu, Osei Akoto, Akwasi Acheampong, Eric Jude Goode, and Opoku Gyamfi. Distribution of natural and artificial radioactivity in soils, water and tuber crops. *Environmental Monitoring and Assessment*, 187(6):1–11, 2015.

[18] Augustine Faanu, Oscar Kwaku Adukpo, Charles Kansaana, Lordford Tettey-Larbi, Henry Lawluvi, David Okoh Kpeglo, Emmanuel Ofori Darko, Geoffrey Emi-Reynolds, Razak Abdul Awudu, Peter Atta Amoah,

et al. Impact assessment of naturally occurring radioactive materials on the public from gold mining and processing at newmont golden ridge limited, akyem, eastern region of ghana. *Radiation Protection and Environment*, 39(3):155, 2016.

[19] AC Patra, S Mohapatra, SK Sahoo, P Lenka, JS Dubey, RM Tripathi, and VD Puranik. Age-dependent dose and health risk due to intake of uranium in drinking water from jaduguda, india. *Radiation protection dosimetry*, 155(2):210–216, 2013.

[20] Pia Vesterbacka et al. 238u-series radionuclides in finnish groundwater-based drinking water and effective doses. 2005.

[21] Frank Winde. Uranium pollution of the wonderfonteinspruit, 1997-2008 part 1: Uranium toxicity, regional background and mining-related sources of uranium pollution. *Water Sa*, 36(3):239–256, 2010.

[22] United Nations Scientific Committee on the Effects of Atomic Radiation et al. Sources and effects of ionizing radiation: Unscear 1993 report to the general assembly. *New York, NY: United Nations*, pages 280–283, 1993.

[23] National Research Council et al. Dose reconstruction for the fernald nuclear facility: A review of task 4. 1994.

[24] World Nuclear Association et al. Chernobyl accident 1986. *Retrieved February*, 16:2013, 2012.

[25] William G Myers. Becquerel's discovery of radioactivity in 1896. *Journal of Nuclear Medicine*, 17(7):579–582, 1976.

[26] Jean Becquerel and JA Crowther. Discovery of radioactivity. *Nature*, 161(4094):609, 1948.

[27] A Martínez-Aguirre, M García-León, and M Ivanovich. The distribution of u, th and ra-226 derived from the phosphate fertilizer industries on an estuarine system in southwest spain. *Journal of environmental radioactivity*, 22(2):155–177, 1994.

[28] Norman E Holden, Tyler B Coplen, John K Böhlke, Lauren V Tarbox, Jacqueline Benefield, John R de Laeter, Peter G Mahaffy, Glenda O'Connor, Etienne Roth, Dorothy H Tepper, et al. Iupac periodic table of the elements and isotopes (iptei) for the education community (iupac technical report). *Pure and Applied Chemistry*, 90(12):1833–2092, 2018.

[29] Michael F L'Annunziata. *Handbook of radioactivity analysis*. Academic press, 2012.

[30] USGS Fda. Nist: Multi-agency radiological laboratory analytical protocols manual (marlap), fda, usgs, nureg-1576. Technical report, EPA 402-B-04-001C, NTIS PB2004-105421, Alexandria, VA, USA, 2004.

[31] SG Kadmenskij and VI Furman. Alpha decay and related nuclear reactions. 1985.

[32] Jianmin Dong, Hongfei Zhang, Yanzhao Wang, Wei Zuo, and Junqing Li. Alpha-decay for heavy nuclei in the ground and isomeric states. *Nuclear Physics A*, 832(3-4):198–208, 2010.

[33] Livhuwani Masevhe. *An Analytical Study of Radon Concentration in Water from Some Rivers in Gauteng Using a Solid-State α- Detector*. PhD thesis, University of Johannesburg (South Africa), 2017.

[34] Kenneth S Krane, David Halliday, et al. *Introductory nuclear physics*, volume 465. Wiley New York, 1988.

[35] Moritz Gradmann. *Radioanalytical separation and measurement techniques for uranium in environmental samples*. PhD thesis, Master thesis, institute of earth and environmental sciences, albert-ludwigs ..., 2015.

[36] BD Goldstein, M Eisenbud, TF Gesell, SA Ibrahim, DC Kocher, ER Landa, and AS Paschoa. Evaluation of guidelines for exposures to technologically enhanced naturally occurring radioactive materials. In *Report to the National Academy of Sciences–National Research Council (NAS–NRC)*. National Academy Press Washington, DC, 1999.

[37] Attila Vértes, Sándor Nagy, Zoltán Klencsár, Rezso György Lovas, and Frank Rösch. *Handbook of Nuclear Chemistry: Vol. 1: Basics of Nuclear Science; Vol. 2: Elements and Isotopes: Formation, Transformation, Distribution; Vol. 4: Radiochemistry and Radiopharmaceutical Chemistry in Life Sciences; Vol. 5: Instrumentation, Separation Techniques, Environmental Issues;*. Springer Science & Business Media, 2010.

[38] S Meroli. Interaction of radiation with matter: from the theory to the measurements. 2012.

[39] Glenn F Knoll. *Radiation detection and measurement*. John Wiley & Sons, 2010.

[40] United Nations Scientific Committee on the Effects of Atomic Radiation et al. Ionizing radiation, sources and biological effects, united nations scientific committee on the effects of atomic radiation (unscear) 1982 report: Report to the general assembly, with scientific annexes. 1982.

[41] James E Parks. The compton effect-compton scattering and gamma ray spectroscopy. *Department of Physics and Astronomy, The University of Tennessee Knoxville, Tennessee*, pages 37996–1200, 2015.

[42] Saman Khabbat Ezzulddin and Habeeb Hanna Mansour. Radon and radium activity concentration measurement in drinking water resources in kurdistan region-iraq. *Journal of Radioanalytical and Nuclear Chemistry*, 324(3):963–976, 2020.

[43] Matthew Veale. *Charge transport and low temperature phenomena in single crystal CdZnTe*. University of Surrey (United Kingdom), 2009.

[44] SO Achola, JP Patel, HK Angeyo, and AO Mustapha. Natural radioactivity and associated radiation characteristic of the new high background radiation area of lambwe east southern kenya. 2010.

[45] Jolyon H Hendry, Steven L Simon, Andrzej Wojcik, Mehdi Sohrabi, Werner Burkart, Elisabeth Cardis, Dominique Laurier, Margot Tirmarche, and Isamu Hayata. Human exposure to high natural background radiation: what can it teach us about radiation risks? *Journal of Radiological Protection*, 29(2A):A29, 2009.

[46] United Nations. Scientific Committee on the Effects of Atomic Radiation. *Sources and effects of ionizing radiation: sources*, volume 1. United Nations Publications, 2000.

[47] Abdelhamid H Elgazzar and Nafisa Kazem. Biological effects of ionizing radiation. In *The pathophysiologic basis of nuclear medicine*, pages 715–726. Springer, 2015.

[48] United Nations Scientific Committee on the Effects of Atomic Radiation et al. Sources, effects and risks of ionizing radiation. 1988.

[49] Radiological Protection. Icrp publication 103. *Ann ICRP*, 37(2.4):2, 2007.

[50] Cristina Nuccetelli, Rosella Rusconi, and Maurizio Forte. Radioactivity in drinking water: regulations, monitoring results and radiation protection issues. *Annali dell'Istituto superiore di sanità*, 48:362–373, 2012.

[51] Aziz Ahmed Qureshi, Shahina Tariq, Kamal Ud Din, Shahid Manzoor, Chiara Calligaris, and Abdul Waheed. Evaluation of excessive lifetime cancer risk due to natural radioactivity in the rivers sediments of northern pakistan. *Journal of Radiation Research and Applied Sciences*, 7(4):438–447, 2014.

[52] Soma Giri and VN Jha. Risk assessment (chemical and radiological) due to intake of uranium through the ingestion of drinking water around two proposed uranium mining areas, jharkhan d, india. *Radioprotection*, 47(4):543–551, 2012.

[53] Bjinse T Dankert and Kim AA Hein. Evaluating the structural character and tectonic history of the witwatersrand basin. *Precambrian Research*, 177(1-2):1–22, 2010.

[54] Randfontein WEST RAND DISTRICT. West rand district municipality draft integrated development plan 2016/17 to 2020/21 revised in 2020/21 preparedin-house. *WEST RAND DISTRICT MUNICIPALITY. Available from: http://www.wrdm.gov.za/wp-content/uploads/2020/04/DRAFT-IDP-2020-21-v4.pdf*, 2016.

[55] Neil MacKellar, Mark New, and Chris Jack. Observed and modelled trends in rainfall and temperature for south africa: 1960-2010. *South African Journal of Science*, 110(7-8):1–13, 2014.

[56] Mohamed M ElBaradei, Mohamed El Baradei, and Werner Burkart. *Handbook of radioactivity analysis*. Academic Press, 2003.

[57] SABS. South african national standard 241-1: Drinking water part 1: Microbiological, physical, aesthetic and chemical determinands, 2011.

[58] Oana Alexandra Dumitru, R. Cs Begy, D.C Nita, L.D. Bobos, and C. Cosma. Uranium electrodeposition for alpha spectrometric source preparation. *Journal of Radioanalytical and Nuclear Chemistry*, 298(2):1335–1339, 2013.

[59] Lyndsey Renee Kelly. Optimization of the microprecipitation procedure for nuclear forensics applications. 2009.

[60] FE Stanley, SE Glover, AM Stalcup, HB Spitz, and Donna Beals. Alpha spectrometric evaluation of srm-995 as a potential uranium/thorium

double tracer system for age-dating uranium materials. *Journal of Radioanalytical and Nuclear Chemistry*, 296(2):1085–1090, 2013.

[61] Xuejin Liu, Hans Bornefalk, Han Chen, Mats Danielsson, Staffan Karlsson, Mats Persson, Cheng Xu, and Ben Huber. A silicon-strip detector for photon-counting spectral ct: energy resolution from 40 kev to 120 kev. *IEEE Transactions on Nuclear Science*, 61(3):1099–1105, 2014.

[62] H Michel, D Levent, V Barci, G Barci-Funel, and C Hurel. Sequential determination of natural (232 th, 238 u) and anthropogenic (137 cs, 90 sr, 241 am, 239+ 240 pu) radionuclides in environmental matrix. 2008.

[63] H Kikunaga, Y Kasamatsu, K Takamiya, T Ohtsuki, H Yuki, A Yokoyama, T Nakanishi, and T Mitsugashira. Development of a rapid source preparation method for high-resolution α-particle spectrometry. *Applied Radiation and Isotopes*, 67(4):539–543, 2009.

[64] Nóra Vajda, Roy Pöllänen, Paul Martin, and Chang-Kyu Kim. Alpha spectrometry. In *Handbook of radioactivity analysis*, pages 493–573. Elsevier, 2020.

[65] D Coomber. *Radiochemical methods in analysis*. Springer Science & Business Media, 2012.

[66] MR Calin, MA Saizu, I Radulescu, and AE Druker. Experimental characterization of a multi-chamber alpha spectrometry system using standard actinide sources. *Nuclear Instruments and Methods in Physics Research Section A: Accelerators, Spectrometers, Detectors and Associated Equipment*, 705:13–16, 2013.

[67] *Analytical Methodology for the Determination of Radium Isotopes in Environmental Samples*. Number 19 in Analytical Quality in Nuclear Applications Series. INTERNATIONAL ATOMIC ENERGY AGENCY, Vienna, 2011.

[68] Robert M Parr and Eduardo Cortes-Toro. Applications of nuclear analytical methods in the life sciences as exemplified by recent research programs of the iaea. *Nuclear Analytical Methods in the Life Sciences*, pages 671–681, 1990.

[69] Suresh Kumar Aggarwal. Alpha-particle spectrometry for the determination of alpha emitting isotopes in nuclear, environmental and biological

samples: past, present and future. *Analytical methods*, 8(27):5353–5371, 2016.

[70] Denise B Pelowitz et al. Mcnp6 user's manual. version 1.0. Technical report, Report LA-CP-13-00634, Rev. 0, Los Alamos National Laboratory, USA, 2013.

[71] Isabela M de S Ferreira, Marcelo X de Castro, Valdir dos S Fidelis, and Osvaldir P Santos. Development and validation of an icp-ms method applied to the determination of uranium in urine. 2013.

[72] Scott C Wilschefski and Matthew R Baxter. Inductively coupled plasma mass spectrometry: introduction to analytical aspects. *The Clinical Biochemist Reviews*, 40(3):115, 2019.

[73] Nelida H Serdeiro and Ana DR Grinman. Determination of uranium, plutonium and americium in water using eichrom resins.

[74] MR Calin, MA Saizu, and I Radulescu. Assessments on energy and efficiency calibration of an alpha spectrometry system using standard sources. *Journal of Radioanalytical and Nuclear Chemistry*, 298(1):55–60, 2013.

[75] S Greenfield. Inductively coupled plasmas in atomic fluorescence spectrometry. a review. *Journal of Analytical Atomic Spectrometry*, 9(5):565–592, 1994.

[76] J.W. Poston. Dosimetry. In Robert A. Meyers, editor, *Encyclopedia of Physical Science and Technology (Third Edition)*, pages 603–650. Academic Press, New York, third edition edition, 2003.

[77] Dan Green. *The physics of particle detectors*, volume 12. Cambridge University Press, 2000.

[78] Bernd Kahn. *Radioanalytical chemistry*. Springer Science & Business Media, 2007.

[79] Wafaa F Bakr et al. Analytical method validation of gamma spectrometric procedure for the determination of γ-emitters in environmental samples. *Arab Journal of Nuclear Science and Applications*, 47(3):130–138, 2014.

[80] Kenneth W Edwards. Isotopic analysis of uranium in natural waters by alpha spectrometry. Technical report, USGPO,, 1968.

[81] S Pommé. Typical uncertainties in alpha-particle spectrometry. *Metrologia*, 52(3):S146, 2015.

[82] Kim Hodgson and Leonardo Manus. A drinking water quality framework for south africa. *Water SA*, 32(5), 2006.

[83] Tsewu Ayabulela. Radioactivity assessment of radium and radon concentrations in water sources at and near selected former uranium mines in the west-rand area of johannesburg. Master's thesis, University of the Witwatersrand, 2021.

[84] United Nations Scientific Committee on the Effects of Atomic Radiation et al. *Sources, Effects and Risks of Ionizing Radiation, United Nations Scientific Committee on the Effects of Atomic Radiation (UNSCEAR) 2016 Report: Report to the General Assembly, with Scientific Annexes*. United Nations, 2017.

[85] National nuclear regulator act 1999, act 47 of 1999, and regulations. [Online; accessed 20-December-2021].

[86] Katharina Kern. New standards for the chemical quality of water in europe under the new directive 2013/39/eu. *Journal for European Environmental & Planning Law*, 11(1):31–48, 2014.

[87] NG Part. Radiation protection and safety of radiation sources international basic safety standards. 2011.

[88] DWAF (Department of Water Affairs and Forestry). Radioactivity dose calculation and water quality evaluation guideline for domestic water use. 2002.

Appendix A

Anova Analysis

Table A.1: Uranium 234 activity concentration (mBq/l) from June 2019 to March 2020 in water samples.

Data Summary (Uranium 234 Activity Conc in mBq/l)				
Groups	N	Mean	Std. Dev.	Std. Error
Jun-19	11	625.5455	425.9764	128.4367
Sep-19	11	635.2727	327.4795	98.7388
Dec-19	11	620.7273	436.4257	131.5873
Mar-21	11	497.2727	315.9101	95.2505

Anova Summary (Uranium Isotopes June2019)					
Source	DF	Sum of Square	Mean Square	F-Stats	P value
Between Groups	2	2511364,837	1255682,42	10,7074	0,0003
Within groups	30	3518170,104	117272,337		
Total	32	6029534,941			

Table A.2: Uranium 238 activity concentration (mBq/l) from June 2019 to March 2020 in water samples.

Data Summary (Uranium 238 Activity Conc in mBq/l)				
Groups	N	Mean	Std. Dev.	Std. Error
Jun-19	11	594.7273	412.363	124.3321
Sep-19	11	479.69	377.7992	113.9108
Dec-19	11	488.2645	412.8304	124.473
Mar-21	11	484.4545	303.4229	91.4855

Anova Summary (Uranium isotopes September 2019)					
Source	DF	Sum of Square	Mean Square	F-Stats	P value
Between Groups	2	2210980.151	1105490.076	13.2557	0.0001
Within groups	30	2501926.209	83397.5403		
Total	32	4712906.361			

Anova Summary (Uranium isotopes December 2019)					
Source	DF	Sum of Square	Mean Square	F-Stats	P value
Between Groups	2	2148993.718	1074496.859	8.9221	0.0009
Within groups	30	3612910.046	120430.3349		
Total	32	5761903.765			

Anova Summary (Uranium isotopes March 2020)					
Source	DF	Sum of Square	Mean Square	F-Stats	P value
Between Groups	2	1610182.337	805091.2	12.5759	0.0001
Within groups	30	1920551.841	64018.39		
Total	32	3530734.178			

Table A.3: Uranium 235 activity concentration (mBq/l) from June 2019 to March 2020 in water samples.

Data Summary (Uranium 235 Activity Conc in mBq/l)				
Groups	N	Mean	Std. Dev.	Std. Error
Jun-19	11	25.5455	17.829	5.3756
Sep-19	11	25.1818	14.75	4.4473
Dec-19	11	25.4545	19.8664	5.9899
Mar-21	11	22.4118	3.8035	4.1619

Table A.4: Calculated annual effective dose in mSv/a June 2019.

Data Summary (Uranium isotopes Dose rate June 2019))				
Groups	**N**	**Mean**	**Std. Dev.**	**Std. Error**
1 Year	11	0.029	0.0195	0.0059
5 years	11	0.0244	0.0164	0.0049
10 years	11	0.0247	0.0166	0.005
15 years	11	0.0348	0.0234	0.0071
Adult	11	0.0273	0.0183	0.0055

Anova Summary (Uranium Isotopes June 2019)					
Source	DF	Sum of Square	Mean Square	F-Stats	P value
Between Groups	4	0.0008	0.0002	0.5445	0.7038
Within groups	50	0.0181	0.0004		
Total	54	0.0189			

Table A.5: Calculated annual effective dose in mSv/a Sep 2019.

Data Summary (Uranium isotopes dose rate Sep 2019)				
Groups	N	Mean	Std. Dev.	Std. Error
1 Year	11	0.0364	0.0196	0.0059
5 years	11	0.0306	0.0164	0.005
10 years	11	0.031	0.0167	0.005
15 years	11	0.0436	0.0235	0.0071
Adult	11	0.0342	0.0184	0.0055

Anova Summary (Dose rate September 2019)					
Source	DF	Sum of Square	Mean Square	F-Stats	P value
Between Groups	4	0.0012	0.0003	0.8433	0.5044
Within groups	50	0.0182	0.0004		
Total	54	0.0195			

Table A.6: Calculated annual effective dose in mSv/a December 2019.

Data Summary (Uranium isotopes Dose rate December 2019)				
Groups	N	Mean	Std. Dev.	Std. Error
1 Year	11	0.0353	0.0249	0.0075
5 years	11	0.0297	0.0209	0.0063
10 years	11	0.0301	0.0212	0.0064
15 years	11	0.0423	0.0298	0.009
Adult	11	0.0332	0.0234	0.007

Anova Summary (Dose rate December 2019)					
Source	DF	Sum of Square	Mean Square	F-Stats	P value
Between Groups	4	0.0012	0.0003	0.4901	0.743
Within groups	50	0.0294	0.0006		
Total	54	0.0306			

Table A.7: Calculated annual effective dose in mSv/a March 2020.

Data Summary (Uranium isotopes dose rate March 2020)				
Groups	N	Mean	Std. Dev.	Std. Error
1 Year	11	0.0302	0.0189	0.0057
5 years	11	0.0253	0.0159	0.0048
10 years	11	0.0257	0.0161	0.0048
15 years	11	0.0361	0.0226	0.0068
Adult	11	0.0283	0.0177	0.0053

Anova Summary (Dose rate March 2020)					
Source	DF	Sum of Square	Mean Square	F-Stats	P value
Between Groups	4	0.0008	0.0002	0.624	0.6475
Within groups	50	0.0169	0.0003		
Total	54	0.0178			